http://pubs.acs.org/journal/acsodf

Article

Structure Elucidation of 16 Undescribed Steroidal Glycosides from the Underground Parts of *Agapanthus africanus* and Apoptosis-Inducing Activity in Small-Cell Lung Cancer Cell

Naoki Takahashi, Tomoki Iguchi,* Anju Nagamine, Remina Shirai, Akihiro Nagata, Junji Yamauchi, and Yoshihiro Mimaki

Cite This: *ACS Omega* 2023, 8, 2808−2830

ABSTRACT: To explore new candidates for anticancer agents from natural products, the underground parts of *Agapanthus africanus*, commonly used as an ornamental plant, were investigated phytochemically. As a result, 16 undescribed steroidal glycosides (**1**−**16**) were obtained, and their structures were determined mainly by NMR spectroscopic analysis and chemical transformations. The cytotoxic activities of the isolated compounds (**1**−**16**) against SBC-3 human small-cell lung cancer cells, A549 human adenocarcinoma cells, and HL-60 human promyelocytic leukemia cells were evaluated using the 3-(4,5-dimethylthiazol-2-yl)-2,5-diphenyl-2-tetrazolium bromide (MTT) assay. Compound **1**, a bisdesmosidic furostanol glycoside, and **10**, a bisdesmosidic spirostanol glycoside, were cytotoxic to all three cell lines with IC_{50} values ranging from 1.2 to 13 μM. As **1** exhibited the most potent cytotoxicity against SBC-3 cells among the isolated compounds, its apoptosis-inducing activity toward SBC-3 cells was examined. Compound **1** arrested SBC-3 cells at the G_2/M phase of the cell cycle and effectively induced apoptosis via an intrinsic pathway accompanied by the dissipation of membrane potential and morphological changes in mitochondria.

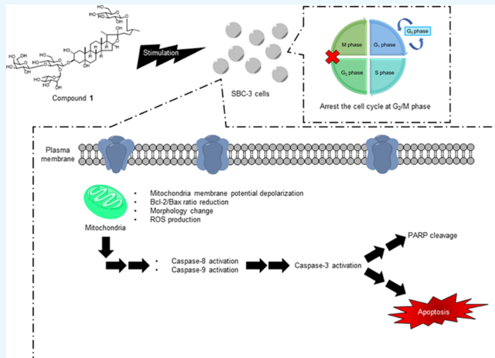

■ INTRODUCTION

Cancer is a major contributor to clinical, social, and economic burdens worldwide. In 2019, there were approximately 24 million new cancer cases and 10 million cancer-related deaths worldwide. Disability-adjusted life years (DALYs) are used as a comprehensive indicator to quantify the overall burden of disease and are calculated from the sum of years of life lost and years lived with disability.[1] Cancer was estimated to have caused approximately 250 million DALYs in 2019.[2] In the DALY ranking of the cancer group, lung, bronchus, and tracheal cancers were the leading causes, with an estimated 46 million DALYs in 2019.[2] To relieve the clinical, social, and economic burden and loss, there is a need to develop novel therapeutic agents for all cancers, including lung cancer. Natural products play a significant role in the development of anticancer agents. Approximately 25% of all new anticancer agents approved by the Food and Drug Administration (FDA) between January 01, 1981, and September 30, 2019, were developed from natural products and natural product derivatives.[3] In our continuous quest for the search for new candidates for anticancer agents from higher plants, we have discovered various cytotoxic steroidal glycosides from *Cestrum nocturnum*,[4] *Ornithogalum thyrsoides*,[5] *Allium karataviense*,[6] *Yucca glauca*,[7] *Dracaena thalioides*,[8] *Ornithogalum saundersiae*,[9] *Convallaria majalis*,[10] *Helleborus foetidus*,[11] *Withania somnifera*,[12] *Thevetia neriifolia*,[13] *Avena sativa*,[14] and *Digitalis purpurea*.[15] Currently, we have focused on the constituents of *Agapanthus africanus* (L.) Hoffmanns. The genus *Agapanthus* consists of seven species, which are mainly distributed in South Africa.[16] As *A. africanus* blooms white or blue flowers, it is now cultivated as an ornamental plant.[17] *A. africanus* is also used as a folk medicine in South Africa to induce or augment labor and treat constipation during pregnancy.[16,18]

Previously, chalcone and dimeric dihydrochalcone derivatives and a steroidal glycoside have been isolated from *A. africanus*.[16,19] However, a literature survey showed that the chemical constituents of *A. africanus* have not been fully investigated, which encouraged us to conduct a detailed phytochemical study on *A. africanus*. Here, we report the isolation and structural characterization of 16 undescribed steroidal glycosides (**1**−**16**) from the underground parts of *A. africanus* and their cytotoxic activities toward SBC-3 human small-cell lung cancer cells, A549 human adenocarcinoma lung cancer cells, and HL-60 human promyelocytic leukemia cells.

Received: December 6, 2022
Accepted: December 28, 2022
Published: January 6, 2023

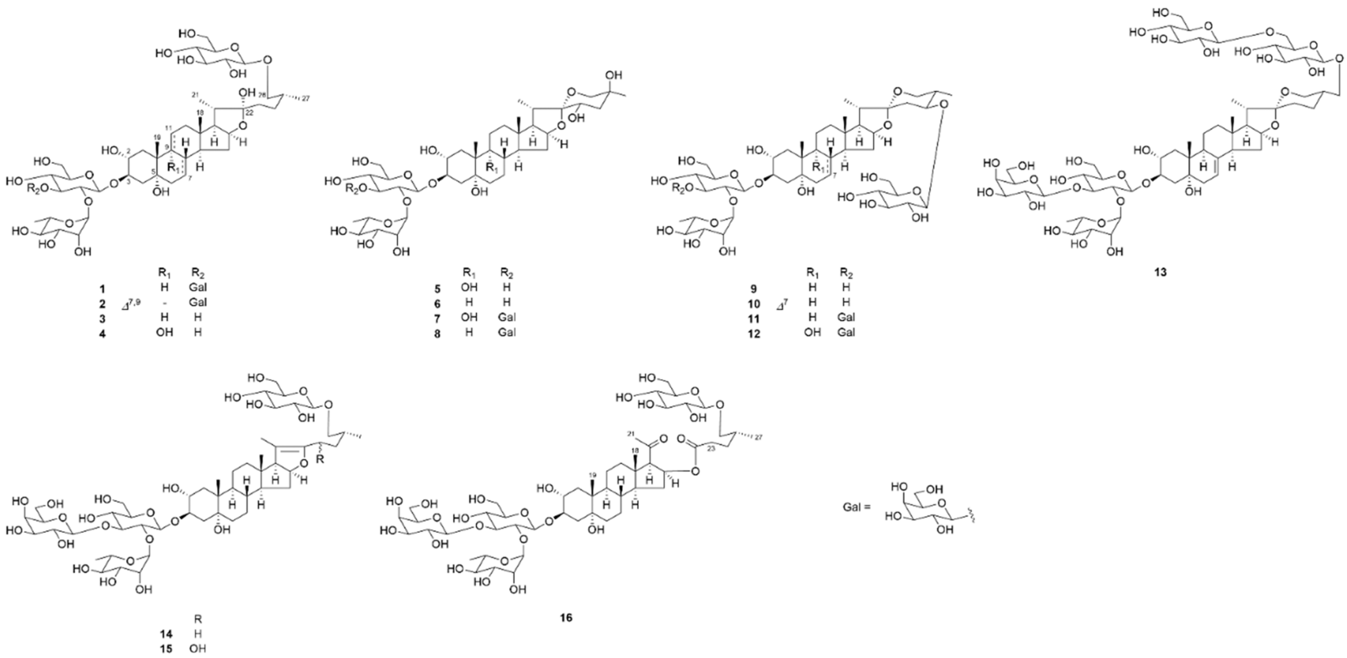

Figure 1. Structures of **1**−**16** isolated from the underground parts of *A. africanus*.

Additionally, the apoptosis-inducing activity of **1** in SBC-3 cells was discussed.

■ RESULTS AND DISCUSSION

Structure Determination. The underground parts of *A. africanus* (fresh weight, 24 kg) were extracted using MeOH (60 °C). After 2 h, the solvent was concentrated under reduced pressure using an evaporator. MeOH extract (910 g) was loaded onto a Diaion HP-20 porous polymer polystyrene resin column and eluted with MeOH/H_2O (3:7), MeOH/H_2O (1:1), MeOH, EtOH, and EtOAc. The MeOH/H_2O (1:1) eluted portion (47 g) was separated by silica gel column chromatography (CC), octadecylsilanized (ODS) silica gel CC, and preparative ODS high-performance liquid chromatography (HPLC) to collect 16 compounds (**1**−**16**) (Figure 1).

Compound **1** was obtained as an amorphous solid, and its molecular formula was identified as $C_{51}H_{86}O_{25}$ based on high-resolution electrospray ionization time-of-flight mass spectroscopy (HRESITOFMS) and ^{13}C nuclear magnetic resonance (NMR) spectral data, which showed an accurate sodium adduct ion at *m/z* 1121.5343 $[M + Na]^+$ (calcd for $C_{51}H_{86}NaO_{25}$: 1121.5356) and 51 carbon signals, respectively. In the ^{1}H and ^{13}C NMR spectra of **1**, the signals for the following functional groups were observed: two tertiary methyl groups [δ_H 1.16 (s, Me-19) and 0.91 (s, Me-18); δ_C 17.2 (C-19) and 16.8 (C-18)], two secondary methyl groups [δ_H 1.30 (d, J = 6.9 Hz, Me-21) and 0.97 (d, J = 6.7 Hz, Me-27); δ_C 17.4 (C-27) and 16.4 (C-21)], three oxygenated methine groups [δ_H 4.92 (q-like, J = 6.9 Hz, H-16), 4.77 (m, H-3), and 4.34 (m, H-2); δ_C 82.7 (C-3), 81.1 (C-16), and 70.9 (C-2)], an oxygenated methylene group [δ_H 3.93 (m, H-26a) and 3.61 (dd, J = 9.5, 6.0 Hz, H-26b); δ_C 75.2 (C-26)], a hemiacetal carbon [δ_C 110.6 (C-22)], an oxygenated quaternary carbon [δ_C 73.6 (C-5)], and four anomeric protons/carbons [δ_H 6.30 (br s), 4.97 (d, J = 7.8 Hz), 4.84 (d, J = 7.7 Hz), and 4.80 (d, J = 7.8 Hz); δ_C 105.1, 104.8, 102.1, and 100.7] (Tables 1 and 5). The NMR spectral data implied that **1** was a furostan-type steroidal glycoside. The enzymatic hydrolysis of **1** with *β*-D-glucosidase yielded (25*R*)-2*α*,5*α*-dihydroxyspirostan-3*β*-yl *O*-*β*-D-galactopyranosyl-(1 → 3)-*O*-[*α*-L-rhamnopyranosyl-(1 → 2)]-*β*-D-glucopyranoside (agapanthussaponin A)[20] and D-glucose. Thus, **1** was identified as the corresponding furostanol glycoside of agapanthussaponin A. In the heteronuclear multiple bond correlation (HMBC) spectrum of **1**, the linkage of a *β*-D-glucopyranosyl [Glc (II): δ_H 4.80 (d, J = 7.8 Hz, H-1⁗); δ_C 104.8, 75.2, 78.5, 71.6, 78.4, and 62.7 (C-1⁗−6⁗)] group to the C-26 hydroxy moiety of the aglycone was confirmed by a $^3J_{C,H}$ correlation between H-1⁗ of Glc (II) and C-26 of the aglycone. The *β*-orientation of the anomeric center of Glc (II) was identified based on the relatively large coupling constant value of H-1⁗ and H-2⁗ (7.8 Hz). Furthermore, the configuration of the C-22 hydroxy group was determined to be *α* based on nuclear Overhauser effect (NOE) correlations between H-20 [δ_H 2.23 (m)] and Me-18/H_2-23 [δ_H 2.05 (m) and 2.01 (m)] in the nuclear Overhauser and exchange spectroscopy (NOESY) spectrum of **1**. Thus, **1** was determined to be (25*R*)-26-[(*β*-D-glucopyranosyl)oxy]-2*α*,5*α*,22*α*-trihydroxyfurostan-3*β*-yl *O*-*β*-D-galactopyranosyl-(1 → 3)-*O*-[*α*-L-rhamnopyranosyl-(1 → 2)]-*β*-D-glucopyranoside.

The ^{1}H and ^{13}C NMR spectra of **2** were similar to those of **1**, except for the signals assigned to the B- and C-ring moieties of the furostan skeleton. The molecular formula of **2** ($C_{51}H_{82}O_{25}$) was smaller than that of **1** by four hydrogen atom, and the signals arising from the two pairs of olefinic groups [δ_H 5.22 (br d, J = 3.9 Hz, H-7); δ_C 117.4 (C-7) and 135.5 (C-8); δ_H 5.73 (br s, H-11); δ_C 142.5 (C-9) and 121.1 (C-11)] were newly observed in the ^{1}H and ^{13}C NMR spectra of **2** (Tables 1 and 5). Additionally, the absorption maxima observed at 243 and 203 nm in the ultraviolet (UV) spectrum are indicative of the existence of conjugated systems in **2**. Enzymatic hydrolysis of **2** was carried out under the same conditions as those used for the hydrolysis of **1** to afford (25*R*)-2*α*,5*α*-dihydroxyspirosta-7,9-dien-3*β*-yl *O*-*β*-D-galactopyranosyl-(1 → 3)-*O*-[*α*-L-rhamnopyranosyl-(1 → 2)]-*β*-D-glucopyranoside (agapanthussaponin C)[20] and D-glucose. A long-range correlation from H-1⁗ of Glc (II) [δ_H 4.80 (d, J = 7.8 Hz)] and C-26 of the aglycone (δ_C 75.2) was observed in the HMBC spectrum of **2**. Accordingly, **2** was

https://doi.org/10.1021/acsomega.2c07766
ACS Omega 2023, 8, 2808−2830

Table 1. ^{1}H NMR Spectral Data of 1−4 in C_5D_5N (δ in ppm, J in Hz)[a]

position	1	2	3	4
1ax	2.24 dd (12.4, 12.1)	2.51 dd (12.3, 12.0)	2.25 dd (12.3, 11.9)	2.84 dd (12.0, 12.0)
eq	2.09 dd (12.4, 5.8)	2.44 dd (12.3, 5.3)	2.08 dd (12.3, 5.5)	2.12 m
2	4.34 m	4.37 m	4.32 m	4.38 m
3	4.77 m	4.69 m	4.73 m	4.73 m
4ax	2.28 dd (13.4, 11.5)	2.28 m	2.29 dd (13.6, 11.6)	2.31 m
eq	2.47 dd (13.4, 5.8)	2.67 dd (13.4, 5.2)	2.50 dd (13.6, 5.7)	2.43 dd (13.6, 5.6)
5	–	–	–	–
6ax	1.70 m	2.46 m	1.69 m	1.70 m
eq	1.59 m	2.28 m	1.58 m	1.65 m
7ax	1.70 m	5.22 br d (3.9)	1.68 m	1.87 m
eq	1.37 m	–	1.35 m	1.25 m
8	1.91 m	–	1.91 m	1.96 m
9	1.90 m	–	1.90 m	–
10	–	–	–	–
11ax	1.32 m	5.73 br s	1.32 m	1.70 m
eq	1.49 m	–	1.49 m	1.79 m
12ax	1.11 m	2.01 m	1.11 m	1.54 m
eq	1.72 m	2.11 m	1.71 m	1.87 m
13	–	–	–	–
14	1.20 m	2.14 m	1.20 m	2.21 m
15ax	1.44 m	1.68 m	1.44 m	1.54 m
eq	2.04 m	2.16 m	2.03 m	2.04 m
16	4.92 q-like (6.9)	4.94 m	4.91 m	5.00 q-like (7.7)
17	1.91 dd (8.3, 6.9)	2.05 m	1.91 dd (8.4, 6.3)	2.08 m
18	0.91 s	0.82 s	0.90 s	0.99 s
19	1.16 s	1.27 s	1.13 s	1.23 s
20	2.23 m	2.27 m	2.22 dd (6.9, 6.3)	2.27 m
21	1.30 d (6.9)	1.28 d (6.8)	1.29 d (6.9)	1.30 d (6.8)
22	–	–	–	–
23a	2.05 m	2.06 m	2.05 m	2.08 m
b	2.01 m	2.02 m	2.00 m	2.03 m
24a	2.03 m	2.03 m	2.03 m	2.06 m
b	1.68 m	1.66 m	1.68 m	1.70 m
25	1.91 m	1.92 m	1.91 m	1.93 m
26a	3.93 m	3.92 dd (9.5, 7.1)	3.93 m	3.93 m
b	3.61 dd (9.5, 6.0)	3.61 dd (9.5, 5.8)	3.61 dd (9.5, 6.0)	3.62 dd (9.4, 6.0)
27	0.97 d (6.7)	0.98 d (6.7)	0.97 d (6.7)	0.98 d (6.7)
position	Glc (I)	Glc (I)	Glc (I)	Glc (I)
1′	4.84 d (7.7)	4.88 d (7.4)	4.91 d (7.2)	4.92 d (7.6)
2′	4.09 dd (8.7, 7.7)	4.11 dd (8.8, 7.4)	4.20 dd (8.9, 7.2)	4.20 dd (8.5, 7.6)
3′	4.05 dd (8.7, 8.7)	4.09 dd (8.8, 8.8)	4.19 dd (8.9, 8.9)	4.19 dd (8.5, 8.5)
4′	3.96 dd (8.7, 8.7)	4.02 dd (9.3, 8.8)	4.12 dd (8.9, 8.9)	4.12 dd (8.5, 8.5)
5′	3.70 m	3.71 ddd (9.3, 5.5, 2.3)	3.78 ddd (8.9, 5.7, 2.2)	3.80 m
6′a	4.35 br d (11.3)	4.33 br d (11.7)	4.45 dd (11.9, 2.2)	4.46 dd (11.5, 2.0)
b	4.14 dd (11.3, 5.1)	4.16 dd (11.7, 5.5)	4.26 dd (11.9, 5.7)	4.27 dd (11.5, 5.6)
position	Rha	Rha	Rha	Rha
1″	6.30 br s	6.33 br s	6.34 d (1.2)	6.35 br s
2″	4.86 dd (3.2, 1.6)	4.88 dd (3.3, 1.3)	4.77 dd (3.3, 1.2)	4.76 dd (3.4, 1.6)
3″	4.54 dd (9.4, 3.2)	4.58 dd (9.4, 3.3)	4.59 dd (9.4, 3.3)	4.58 dd (9.2, 3.4)
4″	4.29 dd (9.4, 9.4)	4.30 dd (9.4, 9.4)	4.33 dd (9.4, 9.4)	4.34 dd (9.2, 9.2)
5″	4.87 m	4.89 m	4.93 m	4.91 m
6″	1.70 d (6.1)	1.70 d (6.2)	1.72 d (6.2)	1.73 d (6.1)
position	Gal	Gal	Glc (II)	Glc (II)
1‴	4.97 d (7.8)	4.99 d (7.8)	4.81 d (7.8)	4.82 d (7.7)
2‴	4.46 dd (9.5, 7.8)	4.47 dd (8.4, 7.8)	4.02 dd (8.5, 7.8)	4.03 dd (8.7, 7.7)
3‴	4.12 dd (9.5, 2.6)	4.13 m	4.25 dd (8.5, 8.5)	4.26 dd (8.7, 8.7)
4‴	4.48 br d (2.6)	4.47 br s	4.24 dd (8.5, 8.5)	4.25 dd (8.7, 8.7)
5‴	4.13 m	4.15 m	3.92 m	3.94 m
6‴a	4.44 dd (10.9, 7.1)	4.45 dd (10.8, 7.1)	4.53 dd (11.9, 2.4)	4.54 dd (11.9, 2.2)
b	4.36 m	4.36 dd (10.8, 5.3)	4.39 dd (11.9, 5.2)	4.39 dd (11.9, 5.3)

https://doi.org/10.1021/acsomega.2c07766
ACS Omega 2023, 8, 2808−2830

Table 1. continued

position	Glc (II)	Glc (II)
1''''	4.80 d (7.8)	4.80 d (7.8)
2''''	4.02 dd (8.5, 7.8)	4.01 dd (8.8, 7.8)
3''''	4.25 dd (8.5, 8.5)	4.25 dd (8.8, 8.8)
4''''	4.23 m	4.22 dd (8.8, 8.8)
5''''	3.93 m	3.93 m
6''''a	4.53 dd (11.9, 2.4)	4.53 dd (11.8, 2.3)
b	4.38 dd (11.9, 5.3)	4.38 dd (11.8, 5.3)

[a] ^{1}H NMR spectra of **1**−**3** were recorded at 500 MHz, and **4** was recorded at 600 MHz.

determined to be (25*R*)-26-[(*β*-D-glucopyranosyl)oxy]-2*α*,5*α*,22*α*-trihydroxyfurosta-7,9-dien-3*β*-yl *O*-*β*-D-galactopyranosyl-(1 → 3)-*O*-[*α*-L-rhamnopyranosyl-(1 → 2)]-*β*-D-glucopyranoside.

The ^{1}H and ^{13}C NMR spectra of **3** ($C_{45}H_{76}O_{20}$) were closely related to those of **1**, including the sugar moiety attached to C-26 of the aglycone. However, the molecular formula of **3** is smaller than that of **1** by $C_6H_{10}O_5$, which corresponds to a hexosyl unit. The ^{1}H and ^{13}C NMR, ^{1}H−^{1}H correlation spectroscopy (COSY), and heteronuclear multiple quantum coherence (HSQC) spectra of **3** showed the presence of a terminal *α*-L-rhamnopyranosyl unit [Rha: δ_H 6.34 (d, *J* = 1.2 Hz, H-1″); δ_C 102.0, 72.3, 72.7, 74.1, 69.4, and 18.5 (C-1″−6″)] and a 2-substituted *β*-D-glucopyranosyl unit [Glc (I): δ_H 4.91 (d, *J* = 7.2 Hz, H-1′); δ_C 101.6, 77.8, 79.4, 71.7, 78.1, and 62.3 (C-1′−6′)] as well as a terminal *β*-D-glucopyranosyl unit [Glc (II): δ_H 4.81 (d, *J* = 7.8 Hz, H-1‴); δ_C 104.8, 75.1, 78.5, 71.6, 78.4, and 62.7 (C-1‴−6‴)] attached to C-26 of the aglycone (Tables 1 and 5). The HMBC spectrum of **3** exhibited $^3J_{C,H}$ correlations between H-1″ of Rha and C-2′ of Glc (I), H-1′ of Glc (I) and C-3 of the aglycone (δ_C 83.5), and between H-1‴ of Glc (II) and C-26 of the aglycone (δ_C 75.2). Therefore, **3** was determined to be (25*R*)-26-[(*β*-D-glucopyranosyl)oxy]-2*α*,5*α*,22*α*-trihydroxyfurostan-3*β*-yl *O*-*α*-L-rhamnopyranosyl-(1 → 2)-*β*-D-glucopyranoside.

The ^{1}H and ^{13}C NMR spectral data of **4** ($C_{45}H_{76}O_{21}$) implied that **4** was analogous to **3**, including the sugar moieties attached to the C-3*β* and C-26 hydroxy groups of the aglycone moiety, whereas the molecular formula of **4** was larger than that of **3** by one oxygen atom. Comparison of the ^{1}H and ^{13}C NMR spectra of **4** with those of **3** revealed that the methine carbon signal (δ_C 45.5) attributable to C-9 in **3** was replaced by an oxygenated quaternary carbon signal (δ_C 77.4) in **4** (Table 5). This was supported by HMBC correlations from H-1eq (δ_H 2.12)/H-7eq (δ_H 1.25) to C-9. Thus, **4** was determined to be (25*R*)-26-[(*β*-D-glucopyranosyl)oxy]-2*α*,5*α*,9*α*,22*α*-tetrahydroxyfurostan-3*β*-yl *O*-*α*-L-rhamnopyranosyl-(1 → 2)-*β*-D-glucopyranoside.

Compound **5** was obtained as an amorphous solid. The molecular formula was assigned as $C_{39}H_{64}O_{17}$ based on the HRESITOFMS data [*m/z* 827.4048 $[M + Na]^+$ (calcd for $C_{39}H_{64}NaO_{17}$: 827.4041)] and ^{13}C NMR spectrum (39 carbon signals). The ^{1}H and ^{13}C NMR spectra of **5** displayed signals for three tertiary methyl groups [δ_H 1.26 (s, Me-27), 1.16 (s, Me-19), and 1.12 (s, Me-18); δ_C 26.8 (C-27), 20.1 (C-19), and 16.1 (C-18)], a secondary methyl group [δ_H 1.19 (d, *J* = 7.0 Hz, Me-21); δ_C 14.7 (C-21)], four oxygenated methine groups [δ_H 4.75 (q-like, *J* = 7.0 Hz, H-16), 4.72 (m, H-3), 4.60 (dd, *J* = 11.7, 4.9 Hz, H-23), and 4.37 (m, H-2); δ_C 82.8 (C-3), 82.0 (C-16), 70.9 (C-2), and 64.5 (C-23)], an oxygenated methylene group [δ_H 3.92 (d, *J* = 11.4 Hz, H-26ax) and 3.69 (d, *J* = 11.4 Hz, H-26eq); δ_C 69.1 (C-26)], three oxygenated quaternary carbons [δ_C 77.4 (C-9), 76.7 (C-5), and 69.8 (C-25)], an acetal carbon [δ_C 112.0 (C-22)], and two anomeric protons/carbons [δ_H 6.32 (br s) and 4.90 (d, *J* = 7.5 Hz); δ_C 102.0 and 101.2] (Tables 2 and 5). In the ^{1}H and ^{13}C NMR spectra of **5**, the signals assignable to the A−C ring moieties and diglycosyl group attached to the C-3*β* hydroxy group of the steroidal skeleton were observed at almost the same positions as those of **4**, indicating the presence of the 2*α*-, 5*α*-, and 9*α*-hydroxy groups, and 3*β*-[*O*-*α*-L-rhamnopyranosyl-(1 → 2)-*β*-D-glucopyranosyl]oxy group in **5**. In contrast, long-range correlations were observed from H-23/H-26ax/H-26eq to C-22 in the HMBC spectrum of **5** (Figure 2), which implied that **5** was a spirostan-type steroidal glycoside. In the HMBC spectrum of **5**, the methyl singlet signal assignable to Me-27 (δ_H 1.26) exhibited $^2J_{C,H}$ and $^3J_{C,H}$ correlations with the signals for the methylene carbon (C-24), oxygenated quaternary carbon (C-25), and oxygenated methylene carbon (C-26) (Figure 2). Analysis of the ^{1}H−^{1}H COSY spectrum of **5** revealed that the oxygenated methine proton (H-23) had spin-coupling correlations with the methylene protons [δ_H 2.47 (dd, *J* = 12.1, 4.8 Hz, H-24eq) and 2.28 (dd, *J* = 12.1, 11.7 Hz, H-24ax)]. These data suggest that two additional hydroxy groups are located at C-23 and C-25 of the aglycone. The configurations of the C-23 and C-25 hydroxy groups were determined to be 23*S* and 25*S*, respectively, based on the NOE correlations between H-23 and H-20 [δ_H 3.13 (dd, *J* = 7.0, 6.8 Hz)]/H-24eq, and between H-24ax and H-26ax/Me-27. Therefore, **5** was determined to be (23*S*,25*S*)-2*α*,5*α*,9*α*,23,25-pentahydroxyspirostan-3*β*-yl *O*-*α*-L-rhamnopyranosyl-(1 → 2)-*β*-D-glucopyranoside.

The ^{1}H and ^{13}C NMR spectral features of **6** ($C_{39}H_{64}O_{16}$) resembled those of **5**. However, the molecular formula of **6** was smaller than that of **5** by an oxygen atom. When the ^{13}C NMR spectrum of **6** was compared with that of **5**, the oxygenated carbon signal (δ_C 77.4) attributed to C-9 in **5** was replaced by the methine carbon signal (δ_C 45.5) in **6**, indicating the lack of a hydroxyl group at C-9 in **6** (Table 5). Thus, **6** was determined to be (23*S*,25*S*)-2*α*,5*α*,23,25-tetrahydroxyspirostan-3*β*-yl *O*-*α*-L-rhamnopyranosyl-(1 → 2)-*β*-D-glucopyranoside.

A comparison of the ^{1}H and ^{13}C NMR spectra of **7** ($C_{45}H_{74}O_{22}$) and **8** ($C_{45}H_{74}O_{21}$) with those of **5** and **6** revealed that **7** and **8** had the same aglycone as **5** and **6**, respectively. Each molecular formula of **7** and **8** was larger than that of **5** and **6** by $C_6H_{10}O_5$, and the ^{1}H and ^{13}C NMR, ^{1}H−^{1}H COSY, and HSQC spectra of **7** and **8** showed the signals assignable to a terminal *β*-D-galactopyranosyl unit (Gal) [**7**: δ_H 4.96 (d, *J* = 7.7 Hz, H-1‴ of Gal); δ_C 105.1, 72.4, 75.1, 69.9, 77.3, and 62.0 (C-1‴−6‴ of Gal); **8**: δ_H 4.97 (d, *J* = 7.8 Hz, H-1‴ of Gal); δ_C 105.1, 72.4, 75.2, 69.9, 77.3, and 62.0 (C-1‴−6‴ of Gal)] in addition to the signals for a 2,3-disubstituted *β*-D-glucopyranosyl unit (Glc) and a terminal *α*-L-rhamnopyranosyl unit (Rha) as in **1** and **2** (Tables 2 and 6). In the HMBC spectra of **7** and **8**, $^3J_{C,H}$ correlations were observed between H-1‴ of Gal and C-3′ of

Table 2. [1]H NMR Spectral Data of 5−8 in C_5D_5N (δ in ppm, J in Hz)[a]

position	5	6	7	8
1ax	2.82 dd (12.2, 12.0)	2.25 dd (12.5, 11.6)	2.82 dd (12.2, 12.2)	2.26 dd (12.6, 11.5)
eq	2.09 m	2.06 dd (12.5, 5.5)	2.10 m	2.07 dd (12.6, 5.6)
2	4.37 m	4.32 m	4.38 m	4.33 m
3	4.72 m	4.74 m	4.76 m	4.78 m
4ax	2.25 m	2.28 m	2.24 m	2.26 dd (12.1, 11.9)
eq	2.42 dd (13.6, 5.7)	2.49 m	2.40 dd (13.6, 5.8)	2.48 m
5	–	–	–	–
6ax	1.62 m	1.58 m	1.64 m	1.60 m
eq	1.57 m	1.54 m	1.59 m	1.55 m
7ax	1.90 m	1.69 m	1.93 m	1.73 m
eq	1.24 m	1.34 m	1.26 m	1.36 m
8	1.92 m	1.63 m	1.94 m	1.65 m
9	–	1.89 m	–	1.90 m
10	–	–	–	–
11ax	1.67 m	1.27 m	1.68 m	1.29 m
eq	1.75 m	1.46 m	1.76 m	1.47 m
12ax	1.51 m	1.11 m	1.51 m	1.13 m
eq	1.88 m	1.70 m	1.89 m	1.71 m
13	–	–	–	–
14	2.24 m	1.24 m	2.24 m	1.25 m
15ax	1.65 m	1.55 m	1.66 m	1.57 m
eq	2.11 m	2.10 m	2.12 m	2.12 m
16	4.75 q-like (7.0)	4.68 q-like (7.2)	4.77 m	4.69 q-like (7.0)
17	2.06 m	1.91 dd (7.2, 7.0)	2.08 m	1.92 dd (7.0, 7.0)
18	1.12 s	1.05 s	1.13 s	1.06 s
19	1.16 s	1.08 s	1.17 s	1.10 s
20	3.13 dd (7.0, 6.8)	3.10 dd (7.0, 7.0)	3.13 dd (7.0, 7.0)	3.10 dd (7.0, 7.0)
21	1.19 d (7.0)	1.20 d (7.0)	1.19 d (7.0)	1.20 d (7.0)
22	–	–	–	–
23	4.60 dd (11.7, 4.9)	4.59 dd (11.7, 4.8)	4.60 dd (11.6, 4.9)	4.59 dd (11.7, 4.9)
24ax	2.28 dd (12.1, 11.7)	2.25 m	2.28 dd (12.1, 12.1)	2.27 m
eq	2.47 dd (12.1, 4.8)	2.46 m	2.47 m	2.46 m
25	–	–	–	–
26ax	3.92 d (11.4)	3.92 d (11.4)	3.93 d (11.6)	3.92 d (11.3)
eq	3.69 d (11.4)	3.69 d (11.4)	3.69 d (11.6)	3.70 d (11.3)
27	1.26 s	1.26 s	1.26 s	1.26 s
position	Glc	Glc	Glc	Glc
1′	4.90 d (7.5)	4.90 d (7.4)	4.82 d (7.3)	4.84 d (7.6)
2′	4.19 dd (8.6, 7.5)	4.18 dd (9.1, 7.4)	4.07 dd (8.8, 7.3)	4.09 dd (8.9, 7.6)
3′	4.18 dd (8.6, 8.6)	4.19 dd (9.1, 9.1)	4.04 dd (8.8, 8.8)	4.04 dd (8.9, 8.9)
4′	4.11 dd (8.6, 8.6)	4.11 dd (9.1, 9.1)	3.94 dd (8.8, 8.8)	3.95 dd (8.9, 8.9)
5′	3.79 m	3.77 ddd (9.1, 5.6, 2.3)	3.71 m	3.69 m
6′a	4.44 dd (11.8, 2.2)	4.43 dd (11.8, 2.3)	4.34 br d (11.0)	4.36 m
b	4.26 dd (11.8, 5.8)	4.26 dd (11.8, 5.6)	4.12 m	4.13 dd (11.6, 5.4)
position	Rha	Rha	Rha	Rha
1″	6.32 br s	6.32 d (1.3)	6.29 br s	6.29 d (1.4)
2″	4.76 br s	4.77 dd (3.4, 1.3)	4.85 br d (3.4)	4.86 dd (3.4, 1.4)
3″	4.57 dd (9.4, 3.1)	4.58 dd (9.4, 3.4)	4.52 dd (9.4, 3.4)	4.54 dd (9.4, 3.4)
4″	4.34 dd (9.4, 9.4)	4.33 dd (9.4, 9.4)	4.29 dd (9.4, 9.4)	4.29 dd (9.4, 9.4)
5″	4.89 m	4.92 m	4.83 m	4.85 m
6″	1.71 d (6.2)	1.71 d (6.2)	1.69 d (6.2)	1.69 d (6.2)
position			Gal	Gal
1‴			4.96 d (7.7)	4.97 d (7.8)
2‴			4.45 dd (9.1, 7.7)	4.46 dd (9.6, 7.8)
3‴			4.13 m	4.13 m
4‴			4.48 br d (3.1)	4.49 br d (3.2)
5‴			4.14 m	4.14 m
6‴a			4.44 dd (10.9, 7.0)	4.44 dd (11.3, 7.1)
b			4.35 br d (10.9)	4.35 m

[a][1]H NMR spectra of **6** and **8** were recorded at 500 MHz, and **5** and **7** were recorded at 600 MHz.

https://doi.org/10.1021/acsomega.2c07766
ACS Omega 2023, 8, 2808−2830

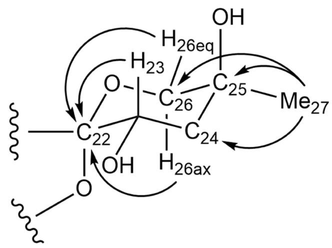

Figure 2. Important HMBC correlations of the F-ring part of **5**.

Glc, H-1″ of Rha and C-2′ of Glc, and between H-1′ of Glc and C-3 of the aglycone (**7**: δ_C 82.1; **8**: δ_C 82.6). Accordingly, **7** and **8** were determined to be (23*S*,25*S*)-2*α*,5*α*,9*α*,23,25-pentahydroxyspirostan-3*β*-yl *O*-*β*-D-galactopyranosyl-(1 → 3)-*O*-[*α*-L-rhamnopyranosyl-(1 → 2)]-*β*-D-glucopyranoside and (23*S*,25*S*)-2*α*,5*α*,23,25-tetrahydroxyspirostan-3*β*-yl *O*-*β*-D-galactopyranosyl-(1 → 3)-*O*-[*α*-L-rhamnopyranosyl-(1 → 2)]-*β*-D-glucopyranoside, respectively.

The ^{1}H and ^{13}C NMR spectra of **9** ($C_{45}H_{74}O_{20}$) were essentially analogous to those of **6**, except for the signals arising from the F-ring of the spirostan-type steroidal skeleton. In the ^{1}H−^{1}H COSY spectrum of **9**, the multiplet signal [δ_H 1.88 (m)] assignable to H-25 exhibited spin-coupling correlations with the signals for an oxygenated methine proton [δ_H 4.02 (ddd, *J* = 12.8, 10.4, 4.6 Hz, H-24)], a pair of oxygenated methylene protons [δ_H 3.61 (dd, *J* = 11.4, 5.2 Hz, H-26eq) and 3.54 (dd, *J* = 11.4, 11.4 Hz, H-26ax)], and a methyl group [δ_H 1.13 (d, *J* = 6.1 Hz, Me-27)]. Furthermore, the oxygenated methine proton (H-24) displayed spin-coupling correlations with the methylene protons [δ_H 2.67 (dd, *J* = 12.8, 4.6 Hz, H-23eq) and 1.95 (dd, *J* = 12.8, 12.8 Hz, H-23ax)] (Tables 3 and 6). Thus, the presence of an oxygen atom at C-24 is evident. The configuration of C-24 was determined to be *S*, based on the NOE correlation observed between H-24 and H-26ax in the NOESY spectrum of **9** and a large spin-coupling constant between H-23ax and H-24 (*J* = 12.8 Hz). Acid hydrolysis of **9** with 1 M HCl (dioxane/H_2O, 1:1) yielded D-glucose and L-rhamnose. Analysis of the ^{1}H and ^{13}C NMR, ^{1}H−^{1}H COSY, and HSQC spectra of **9** showed the presence of a terminal *β*-D-glucopyranosyl unit [Glc (II): δ_H 4.91 (d, *J* = 7.6 Hz, H-1‴); δ_C 106.3, 75.6, 78.5, 71.6, 78.0, and 62.7 (C-1‴−6‴)] in addition to the *O*-*α*-L-rhamnopyranosyl-(1 → 2)-*β*-D-glucopyranosyl group attached to the C-3*β* hydroxy group of the aglycone. The $^3J_{C,H}$ correlation from H-1‴ of Glc (II) to C-24 (δ_C 81.5) of the aglycone in the HMBC spectrum of **9** confirmed that the C-24 oxygen atom had a *β*-D-glucopyranosyl group. Thus, **9** was determined to be (24*S*,25*S*)-24-[(*β*-D-glucopyranosyl)oxy]-2*α*,5*α*-dihydroxyspirostan-3*β*-yl *O*-*α*-L-rhamnopyranosyl-(1 → 2)-*β*-D-glucopyranoside.

The ^{1}H and ^{13}C NMR spectra of **10** ($C_{45}H_{72}O_{20}$) were similar to those of **9**. However, the molecular formula of **10** was smaller than that of **9** by two hydrogen atoms. In the ^{1}H and ^{13}C NMR spectra of **10**, signals arising from a trisubstituted olefinic group [δ_H 5.00 (br d, *J* = 3.5 Hz, H-7); δ_C 138.8 (C-8) and 115.9 (C-7)] were observed (Tables 3 and 6). The olefinic proton (H-7) exhibited spin-coupling correlations with the methylene protons [δ_H 2.29 (br d, *J* = 16.4 Hz, H-6a)/2.08 (dd, *J* = 16.4, 3.5 Hz, H-6b)] in the ^{1}H−^{1}H COSY spectrum and long-range correlations with the methine carbons [δ_C 43.3 (C-9) and 54.9 (C-14)] in the HMBC spectrum. These data indicate the presence of a double bond between C-7 and C-8. Therefore, **10** was determined to be (24*S*,25*S*)-24-[(*β*-D-glucopyranosyl)oxy]-2*α*,5*α*-dihydroxyspirost-7-en-3*β*-yl *O*-*α*-L-rhamnopyranosyl-(1 → 2)-*β*-D-glucopyranoside.

Comparison of the ^{1}H and ^{13}C NMR spectra of **11** ($C_{51}H_{84}O_{25}$) with those of **9** indicated that **9** and **11** shared the same aglycone with a (*β*-D-glucopyranosyl)oxy moiety at C-24. However, **11** differed from **9** in the structure of the sugar moiety attached to the C-3*β* hydroxyl group of the aglycone moiety. Analysis of the ^{1}H and ^{13}C NMR, ^{1}H−^{1}H COSY, HSQC, and HMBC spectra of **11** implied that **11** had a branched triglycoside, *O*-*β*-D-galactopyranosyl-(1 → 3)-*O*-[*α*-L-rhamnopyranosyl-(1 → 2)]-*β*-D-glucopyranosyl at the C-3*β* hydroxy group of the aglycone, similar to the concomitantly isolated compounds **1**, **2**, **7**, and **8**. Thus, **11** was determined to be (24*S*,25*S*)-24-[(*β*-D-glucopyranosyl)oxy]-2*α*,5*α*-dihydroxyspirostan-3*β*-yl *O*-*β*-D-galactopyranosyl-(1 → 3)-*O*-[*α*-L-rhamnopyranosyl-(1 → 2)]-*β*-D-glucopyranoside.

The ^{1}H and ^{13}C NMR spectra of **12** ($C_{51}H_{84}O_{26}$) implied that **12** was analogous to **11**, including sugar moieties attached to the C-3*β* and C-24*S* hydroxy groups of the aglycone. The molecular formula of **12** was larger than that of **11** by an oxygen atom. When the ^{13}C NMR spectrum of **12** was compared with that of **11**, the methine carbon signal (δ_C 45.5) assigned to C-9 in **11** was replaced by an oxygenated quaternary carbon signal (δ_C 77.2) in **12**, implying that **12** had a hydroxy group at C-9*α* (Table 6). Thus, **12** was determined to be (24*S*,25*S*)-24-[(*β*-D-glucopyranosyl)oxy]-2*α*,5*α*,9*α*-trihydroxyspirostan-3*β*-yl *O*-*β*-D-galactopyranosyl-(1 → 3)-*O*-[*α*-L-rhamnopyranosyl-(1 → 2)]-*β*-D-glucopyranoside.

Compound **13** ($C_{57}H_{92}O_{30}$) was obtained as an amorphous solid. The ^{1}H and ^{13}C NMR spectra of **13** suggested that the aglycone of **13** was analogous to that of **10**, showing signals for a hydroxy methine group [δ_H 4.26 (m, H-2); δ_C 70.4 (C-2)], a glycosyloxy methine group [δ_H 4.68 (m, H-3); δ_C 82.5 (C-3)], an oxygenated quaternary carbon [δ_C 73.0 (C-5)], an olefinic group [δ_H 5.07 (br d, *J* = 3.4 Hz, H-7); δ_C 115.9 (C-7) and 139.0 (C-8)], two angular methyl groups [δ_H 0.73 (s, Me-18) and 1.11 (s, Me-19); δ_C 16.4 (C-18) and 19.0 (C-19)], a secondary methyl group [δ_H 1.06 (d, *J* = 6.9 Hz, Me-21); δ_C 14.8 (C-21)], and an acetal carbon [δ_C 109.5 (C-22)]. However, the signals for the C-24 glycosyloxy methine group and C-27 methyl group in **10** were replaced by those for a methylene group [δ_H 1.66 (m, H-24a) and 1.64 (m, H-24b); δ_C 23.8 (C-24)] and an oxygenated methylene group [δ_H 4.00 (m, H-27a) and 3.41 (dd, *J* = 9.9, 8.8 Hz, H-27b); δ_C 72.1 (C-27)], respective, in **13**. The above-mentioned data implied that the aglycone of **13** corresponded to that of **10**, but the glycosyloxy group at C-24 was absent, and the methyl group at C-27 was oxidized in the aglycone of **13** (Tables 4 and 7). The acid hydrolysis of **13** resulted in L-rhamnose, D-galactose, and D-glucose were obtained. The ^{1}H and ^{13}C NMR, ^{1}H−^{1}H COSY, HSQC, and HMBC spectra of **13** indicated that **13** had an *O*-*β*-D-galactopyranosyl-(1 → 3)-*O*-[*α*-L-rhamnopyranosyl-(1 → 2)]-*β*-D-glucopyranosyl at the C-3*β* hydroxy group of the aglycone, as in **1**, **2**, **7**, **8**, **11**, and **12**. Furthermore, signals for a 6-substituted *β*-D-glucopyranosyl unit [Glc (II): δ_H 4.69 (d, *J* = 7.7 Hz, H-1⁗); δ_C 104.9, 75.0, 78.5, 71.5, 77.2, and 70.1 (C-1⁗−6⁗)] and a terminal *β*-D-glucopyranosyl unit [Glc (III): δ_H 5.10 (d, *J* = 7.8 Hz, H-1⁗′); δ_C 105.4, 75.2, 78.4, 71.6, 78.5, and 62.7 (C-1⁗′−6⁗′)] were observed (Tables 4 and 7). In the HMBC spectrum of **13**, $^3J_{C,H}$ correlations were observed between H-1⁗′ of Glc (III) and C-6⁗ of Glc (II), and between H-1⁗ of Glc (II) and C-27 of the aglycone, indicating that an *O*-*β*-D-glucopyranosyl-(1 → 6)-*β*-D-glucopyranosyl group was linked

Table 3. ^{1}H NMR Spectral Data of 9−12 in C_5D_5N (δ in ppm, J in Hz)[a]

position	9	10	11	12
1ax	2.25 dd (12.5, 11.9)	2.23 dd (12.3, 12.0)	2.27 m	2.82 dd (12.1, 11.9)
eq	2.06 dd (12.5, 5.3)	2.14 dd (12.3, 4.9)	2.09 m	2.10 dd (12.1, 5.3)
2	4.33 m	4.24 m	4.36 m	4.39 m
3	4.74 m	4.65 m	4.79 ddd (11.0, 8.9, 5.8)	4.76 m
4ax	2.29 dd (13.4, 12.9)	2.34 dd (11.9, 11.7)	2.28 m	2.26 dd (13.3, 11.7)
eq	2.50 dd (13.4, 5.5)	2.64 dd (11.7, 5.4)	2.47 dd (13.5, 5.8)	2.41 dd (13.3, 5.9)
5	–	–	–	–
6ax (a)	1.68 m	2.29 br d (16.4)	1.71 m	1.69 m
eq (b)	1.59 m	2.08 dd (16.4, 3.5)	1.59 m	1.63 m
7ax	1.68 m	5.00 br d (3.5)	1.71 m	1.87 m
eq	1.32 m	–	1.36 m	1.23 m
8	1.51 m	–	1.54 m	1.90 m
9	1.88 m	2.41 m	1.90 m	–
10	–	–	–	–
11ax	1.26 m	1.50 m	1.28 m	1.64 m
eq	1.46 m	1.56 m	1.48 m	1.75 m
12ax	1.05 m	1.14 m	1.08 m	1.42 m
eq	1.61 m	1.63 m	1.62 m	1.80 m
13	–	–	–	–
14	1.17 m	1.84 m	1.18 m	2.15 m
15ax	1.38 m	1.66 m	1.39 m	1.47 m
eq	1.99 m	1.92 m	2.02 m	1.99 m
16	4.49 m	4.51 q-like (7.1)	4.51 m	4.57 q-like (6.9)
17	1.72 m	1.78 dd (7.1, 6.9)	1.73 m	1.86 m
18	0.77 s	0.68 s	0.79 s	0.84 s
19	1.12 s	1.09 s	1.17 s	1.22 s
20	1.92 m	1.89 m	1.93 m	1.95 m
21	1.02 d (6.9)	1.02 d (6.9)	1.04 d (7.0)	1.01 d (6.7)
22	–	–	–	–
23ax	1.95 dd (12.8, 12.8)	1.95 dd (13.2, 13.0)	1.96 m	1.96 m
eq	2.67 dd (12.8, 4.6)	2.67 dd (13.2, 4.9)	2.68 dd (13.0, 4.8)	2.70 dd (13.0, 4.7)
24	4.02 ddd (12.8, 10.4, 4.6)	4.02 m	4.04 m	4.03 m
25	1.88 m	1.88 m	1.90 m	1.87 m
26ax	3.54 dd (11.4, 11.4)	3.52 dd (11.4, 11.4)	3.56 dd (11.4, 11.4)	3.55 dd (11.5, 11.5)
eq	3.61 dd (11.4, 5.2)	3.60 dd (11.4, 5.1)	3.63 dd (11.4, 5.3)	3.60 dd (11.5, 5.3)
27	1.13 d (6.1)	1.14 d (6.5)	1.14 d (6.5)	1.13 d (6.4)
position	Glc (I)	Glc (I)	Glc (I)	Glc (I)
1′	4.90 d (7.6)	4.93 d (7.5)	4.85 d (7.5)	4.83 d (7.6)
2′	4.20 dd (9.2, 7.6)	4.21 dd (9.1, 7.5)	4.12 dd (8.7, 7.5)	4.08 dd (8.9, 7.6)
3′	4.18 dd (9.2, 9.2)	4.20 dd (9.1, 9.1)	4.07 dd (8.7, 8.7)	4.05 dd (8.9, 8.9)
4′	4.12 dd (9.2, 9.2)	4.15 dd (9.1, 9.1)	3.99 dd (9.5, 8.7)	3.93 dd (8.9, 8.9)
5′	3.77 m	3.78 ddd (9.1, 5.4, 2.2)	3.70 ddd (9.5, 5.8, 2.0)	3.71 m
6′a	4.44 dd (11.9, 1.9)	4.43 dd (12.0, 2.2)	4.35 m	4.36 dd (10.7, 2.7)
b	4.26 dd (11.9, 5.3)	4.28 dd (12.0, 5.4)	4.16 dd (11.9, 5.8)	4.12 br d (10.7)
position	Rha	Rha	Rha	Rha
1″	6.34 br s	6.35 d (1.2)	6.33 br s	6.29 br s
2″	4.77 dd (3.4, 1.3)	4.78 dd (3.4, 1.2)	4.86 dd (3.6, 1.7)	4.85 br s
3″	4.59 dd (9.2, 3.4)	4.61 dd (9.3, 3.4)	4.55 m	4.53 dd (9.4, 3.1)
4″	4.34 dd (9.2, 9.2)	4.34 dd (9.3, 9.3)	4.30 dd (9.2, 9.2)	4.30 dd (9.4, 9.4)
5″	4.93 m	4.94 m	4.87 m	4.84 m
6″	1.72 d (6.2)	1.71 d (6.1)	1.71 d (6.3)	1.70 d (6.2)
position	Glc (II)	Glc (II)	Gal	Gal
1‴	4.91 d (7.6)	4.92 d (7.8)	4.98 d (7.8)	4.97 d (7.7)
2‴	4.05 dd (8.8, 7.6)	4.05 dd (8.8, 7.8)	4.48 dd (9.5, 7.8)	4.45 dd (8.9, 7.7)
3‴	4.21 dd (8.8, 8.8)	4.22 dd (8.8, 8.8)	4.10 dd (9.5, 3.2)	4.13 m
4‴	4.27 dd (8.8, 8.8)	4.27 dd (8.8, 8.8)	4.48 br d (3.2)	4.48 br s
5‴	3.84 m	3.84 ddd (8.8, 5.1, 2.5)	4.15 m	4.14 m
6‴a	4.48 dd (12.0, 2.3)	4.46 dd (11.9, 2.5)	4.46 dd (11.0, 6.9)	4.43 m
b	4.36 dd (12.0, 5.2)	4.35 dd (11.9, 5.1)	4.35 m	4.34 br d (10.9)

https://doi.org/10.1021/acsomega.2c07766
ACS Omega 2023, 8, 2808−2830

Table 3. continued

position	Glc (II)	Glc (II)
1''''	4.92 d (7.7)	4.91 d (7.8)
2''''	4.05 dd (8.9, 7.7)	4.04 m
3''''	4.21 dd (8.9, 8.9)	4.21 dd (8.9, 8.9)
4''''	4.28 dd (9.5, 8.9)	4.26 dd (8.9, 8.9)
5''''	3.85 ddd (9.5, 5.1, 2.9)	3.85 ddd (8.9, 5.2, 2.5)
6''''a	4.55 m	4.50 dd (12.2, 2.5)
b	4.38 dd (11.6, 5.1)	4.36 dd (12.2, 5.2)

[a] ^{1}H NMR spectra of **10** and **11** were recorded at 500 MHz, and **9** and **12** were recorded at 600 MHz.

to the oxygen atom at C-27 in **13**. The NOESY spectrum of **13** exhibited NOE correlations between H-25 (δ_H 2.02) and H-23ax (δ_H 1.59), which allowed the configuration of C-25 to be determined as *S*. Based on all of the data mentioned above, **13** was determined to be (25*S*)-27-[*O*-*β*-D-glucopyranosyl-(1 → 6)-(*β*-D-glucopyranosyl)oxy]-2*α*,5*α*-dihydroxyspirost-7-en-3*β*-yl *O*-*β*-D-galactopyranosyl-(1 → 3)-*O*-[*α*-L-rhamnopyranosyl-(1 → 2)]-*β*-D-glucopyranoside.

The ^{1}H and ^{13}C NMR spectra of **14** ($C_{51}H_{84}O_{24}$) showed features similar to those of **1**. However, the molecular formula of **14** was smaller than that of **1** by H_2O, and the signals assignable to H-17 and Me-21 were observed as a doublet δ_H 1.30 (*J* = 6.9 Hz) and as a singlet (δ_H 1.61), respectively. Furthermore, signals for a pair of olefinic carbons were detected [δ_C 103.6 (C-20) and 152.2 (C-22)] (Tables 4 and 7). These data suggest that **14** is the corresponding $\Delta^{20(22)}$-pseudofurostanol glycoside of **1**. The following chemical transformations were conducted to confirm the structure of **14**. Acetylation of **14** with Ac_2O in pyridine at 28 °C for 24 h gave the corresponding tetradecaacetate (**14a**), which was the same as the product obtained by treating **1** with Ac_2O in pyridine at 130 °C for 3 h (Figure 3). Therefore, **14** was determined to be (25*R*)-26-[(*β*-D-glucopyranosyl)oxy]-2*α*,5*α*-dihydroxyfurost-20(22)-en-3*β*-yl *O*-*β*-D-galactopyranosyl-(1 → 3)-*O*-[*α*-L-rhamnopyranosyl-(1 → 2)]-*β*-D-glucopyranoside.

Compound **15** ($C_{51}H_{84}O_{25}$) was suggested to be a $\Delta^{20(22)}$-pseudofurostanol glycoside closely related to **14** based on the ^{1}H and ^{13}C NMR spectra. However, the molecular formula of **15** was larger than that of **14** by one oxygen atom. In the ^{1}H–^{1}H COSY spectrum of **15**, the methine proton [δ_H 2.47 (m)] attributable to H-25 showed spin-coupling correlations with the methylene protons [δ_H 2.40 (m, H-24a) and 1.78 (ddd, *J* = 13.2, 7.2, 6.0 Hz, H-24b)], oxygenated methylene protons [δ_H 4.05 (m, H-26a) and 3.80 (dd, *J* = 9.6, 5.4 Hz, H-26b)], and methyl protons [δ_H 1.19 (d, *J* = 7.2 Hz, Me-27)]. The methylene protons (H_2-24) in turn showed spin-coupling correlations with the oxygenated methine proton [δ_H 4.92 (dd, *J* = 8.4, 6.0 Hz, H-23)]. These correlations indicate the presence of a hydroxy group at C-23 of the aglycone. The absolute configuration of C-23 remains to be determined, owing to its low yield. As **15** was biosynthesized from **14**, the configuration of C-25 was assumed to be *R*. Accordingly, **15** was determined to be (25*R*)-26-[(*β*-D-glucopyranosyl)oxy]-2*α*,5*α*,23-trihydroxyfurost-20(22)-en-3*β*-yl *O*-*β*-D-galactopyranosyl-(1 → 3)-*O*-[*α*-L-rhamnopyranosyl-(1 → 2)]-*β*-D-glucopyranoside. Pseudofurostanol glycosides with a hydroxy group at C-23 were isolated from *Tribulus terrestris*.[21]

Compound **16** ($C_{51}H_{84}O_{26}$) was obtained as an amorphous solid. The ^{1}H and ^{13}C NMR data for **16** were essentially analogous to those for **14**, except for the lack of signals for the C-20(22)-tetrasubstituted olefinic group. Instead, signals for a keto carbonyl carbon (δ_C 205.5) and an ester carbonyl carbon (δ_C 173.2) were observed in the ^{13}C NMR spectrum of **16** (Table 7). All other signals appeared at almost the same position between the two glycosides. In the HMBC spectrum of **16**, the methine proton [δ_H 2.46 (d, *J* = 11.3 Hz, H-17)] and methyl protons [δ_H 2.10 (s, Me-21)] showed long-range correlations with the keto carbonyl carbon, which was assigned to C-20. Long-range correlations from the oxygenated methine proton [δ_H 5.65 (m, H-16)] and methylene protons [δ_H 2.45 (m, H-23a) and 2.40 (m, H-23b)] to the ester carbonyl carbon resulted in the assignment of the ester carbonyl carbon to C-22. These data suggest that **16** was formed from **14** through the oxidative cleavage of the C-20(22) double bond. This was confirmed by the fact that the peracetate (**16a**) of **16** was identical to the product obtained by treating **14** with Ac_2O in pyridine at 28 °C for 24 h and then with CrO_3 in AcOH at 28 °C for 2.5 h (Figure 3). Therefore, **16** was determined to be 3*β*-[(*O*-*β*-D-galactopyranosyl-(1 → 3)-*O*-[*α*-L-rhamnopyranosyl-(1 → 2)]-*β*-D-glucopyranosyl)oxy]-2*α*,5*α*-dihydroxy-16*β*-[[(4*R*)-5-(*β*-D-glucopyranosyloxy)-4-methyl-1-oxopentyl]oxy]-pregn-5-en-20-one.

Cytotoxic Activities of 1–16. Compounds **1**–**16** were assessed for their cytotoxicity against SBC-3, A549, and HL-60 cells using a modified 3-(4,5-dimethylthiazol-2-yl)-2,5-diphenyl-2-tetrazolium bromide (MTT) assay (Table 8). Compounds **1** and **10** exhibited dose-dependent cytotoxic activities against all three cell lines (Figure 4). The cytotoxic activities of **1** were attenuated by the dehydrogenation of C-7/8 and C-9/11 (**2**), degalactosylation (**3**), and dehydrogenation of C-20/22 (**14**). On the other hand, although **9** did not show any cytotoxicity against the three cell lines at a sample concentration of 50 *μ*M, the C-7/8 dehydro derivative of **9** (**10**) was considerably cytotoxic to all three cell lines.

Apoptosis-Inducing Activity of 1 in SBC-3 Cells. Compound **1** exerted the most potent cytotoxicity against SBC-3 cells among the isolated compounds and was obtained in a good yield. Therefore, **1** was assessed for its apoptosis-inducing activity in the SBC-3 cells. SBC-3 cells were treated with **1** for 24 h to determine the concentration for the apoptosis-inducing activity assay. As a result, the IC_{50} values of **1** and cisplatin were calculated to be 7.9 ± 0.10 and 6.5 ± 0.15 *μ*M, respectively (Figure 5). Thus, the apoptosis-inducing activities of **1** and cisplatin were evaluated at concentrations of 15 and 10 *μ*M, respectively.

After the SBC-3 cells were exposed to **1** for 24 h, they were stained with Annexin V and propidium iodide (PI), and the apoptotic cell ratio was analyzed using a flow cytometer. As shown in Figure 6, the percentage of early (Q4 area) and late (Q2 area) apoptotic cell populations significantly increased to 15.8 ± 0.35 and 30 ± 0.94% for **1**, respectively, compared to 2.5 ± 0.067 and 4.6 ± 0.35% for the vehicle control, respectively (Figure 6). Furthermore, SBC-3 cells treated with **1** for 24 h were stained with 4′,6′-diamidino-2-phenylindole dichloride

https://doi.org/10.1021/acsomega.2c07766
ACS Omega 2023, 8, 2808–2830

Table 4. ^{1}H NMR Spectral Data of 13−16 in C_5D_5N (δ in ppm, J in Hz)[a]

position	13	14	15	16
1ax	2.24 m	2.27 m	2.29 m	2.27 m
eq	2.15 dd (12.6, 5.3)	2.09 m	2.11 m	2.08 dd (12.0, 5.4)
2	4.26 m	4.34 m	4.37 m	4.35 m
3	4.68 m	4.78 m	4.80 m	4.79 m
4ax	2.32 m	2.28 m	2.30 m	2.31 dd (13.7, 11.7)
eq	2.62 dd (13.6, 5.3)	2.47 dd (13.5, 5.7)	2.48 m	2.48 dd (13.7, 5.6)
5	–	–	–	–
6ax	2.28 m	1.72 m	1.75 m	1.78 m
eq	2.10 m	1.61 m	1.61 m	1.62 m
7ax	5.07 br d (3.4)	1.72 m	1.74 m	1.75 m
eq	–	1.37 m	1.39 m	1.37 m
8	–	1.51 m	1.52 m	1.55 m
9	2.42 m	1.88 m	1.90 m	1.92 m
10	–	–	–	–
11ax	1.55 m	1.31 m	1.31 m	1.37 m
eq	1.57 m	1.50 m	1.51 m	1.52 m
12ax	1.15 m	1.13 m	1.14 m	1.10 m
eq	1.66 m	1.71 m	1.70 m	2.16 m
13	–	–	–	–
14	1.83 m	0.97 m	0.96 m	0.94 m
15ax	1.67 m	1.47 m	1.49 m	1.32 m
eq	1.94 m	2.12 m	2.12 m	2.43 m
16	4.47 m	4.74 m	4.78 m	5.65 m
17	1.79 m	2.39 d (10.1)	2.42 d (10.2)	2.46 d (11.3)
18	0.73 s	0.74 s	0.75 s	1.24 s
19	1.11 s	1.16 s	1.17 s	1.18 s
20	1.86 m	–	–	–
21	1.06 d (6.9)	1.61 s	1.74 s	2.10 s
22	–	–	–	–
23ax (a)	1.59 m	2.23 m	4.92 dd (8.4, 6.0)	2.45 m
eq (b)	1.65 m	2.19 m	–	2.40 m
24ax (a)	1.64 m	1.81 m	2.40 m	1.96 m
eq (b)	1.66 m	1.45 m	1.78 ddd (13.2, 7.2, 6.0)	1.56 m
25	2.02 m	1.94 m	2.47 m	1.88 m
26ax (a)	4.03 m	3.93 dd (9.5, 7.1)	4.05 m	3.89 dd (9.6, 6.6)
eq (b)	3.67 m	3.61 dd (9.5, 5.6)	3.80 dd (9.6, 5.4)	3.51 dd (9.6, 6.1)
27a	4.00 m	1.01 d (6.7)	1.19 d (7.2)	0.92 d (6.7)
b	3.41 dd (9.9, 8.8)	–	–	–
position	Glc (I)	Glc (I)	Glc (I)	Glc (I)
1′	4.85 d (7.5)	4.84 d (7.7)	4.87 d (7.6)	4.85 d (7.5)
2′	4.11 dd (8.8, 7.5)	4.09 dd (8.8, 7.7)	4.14 dd (9.0, 7.6)	4.12 dd (8.7, 7.5)
3′	4.07 dd (8.8, 8.8)	4.04 dd (8.8, 8.8)	4.08 dd (9.0, 9.0)	4.06 dd (8.7, 8.7)
4′	4.00 dd (8.8, 8.8)	3.95 dd (9.4, 8.8)	4.00 dd (9.0, 9.0)	3.99 dd (9.4, 8.7)
5″	3.70 m	3.70 ddd (9.4, 5.6, 2.1)	3.72 ddd (9.0, 6.0, 2.4)	3.70 ddd (9.4, 5.7, 2.4)
6′a	4.34 dd (11.8, 2.5)	4.35 dd (11.6, 2.1)	4.39 dd (12.0, 2.4)	4.36 dd (11.8, 2.4)
b	4.15 dd (11.8, 5.0)	4.14 dd (11.6, 5.6)	4.17 dd (12.0, 6.0)	4.16 dd (11.8, 5.7)
position	Rha	Rha	Rha	Rha
1″	6.32 br s	6.29 br s	6.34 br s	6.33 br s
2″	4.85 br d (3.4)	4.84 br s	4.86 br s	4.85 br s
3″	4.56 dd (9.3, 3.4)	4.54 dd (9.1, 3.4)	4.55 dd (9.6, 3.6)	4.54 dd (9.4, 3.5)
4″	4.29 dd (9.3, 9.3)	4.28 dd (9.1, 9.1)	4.30 dd (9.6, 9.6)	4.29 dd (9.4, 9.4)
5″	4.88 m	4.86 m	4.88 m	4.87 m
6″	1.70 d (6.2)	1.69 d (6.2)	1.72 d (6.0)	1.70 d (6.2)
position	Gal	Gal	Gal	Gal
1‴	4.98 d (7.8)	4.96 d (7.8)	4.98 d (7.8)	4.97 d (7.8)
2‴	4.46 dd (9.4, 7.8)	4.45 dd (9.0, 7.8)	4.49 dd (9.0, 7.8)	4.47 dd (9.5, 7.8)
3‴	4.10 dd (9.4, 3.2)	4.10 dd (9.0, 3.1)	4.09 dd (9.0, 3.6)	4.10 dd (9.5, 3.1)
4‴	4.47 br d (3.2)	4.46 br d (3.1)	4.48 br d (3.6)	4.48 br d (3.1)
5‴	4.14 m	4.13 m	4.16 m	4.15 m
6‴a	4.45 dd (10.9, 7.4)	4.44 dd (11.0, 6.7)	4.47 dd (10.8, 7.2)	4.46 dd (11.0, 6.9)

https://doi.org/10.1021/acsomega.2c07766
ACS Omega 2023, 8, 2808−2830

Table 4. continued

position	Gal	Gal	Gal	Gal
b	4.36 dd (10.9, 5.1)	4.35 dd (11.0, 5.1)	4.38 dd (10.8, 5.4)	4.36 dd (11.0, 4.9)
position	Glc (II)	Glc (II)	Glc (II)	Glc (II)
1⁗	4.69 d (7.7)	4.82 d (7.9)	4.88 d (7.7)	4.80 d (7.8)
2⁗	3.95 dd (8.7, 7.7)	4.03 dd (8.7, 7.9)	4.06 dd (9.0, 7.7)	4.02 dd (8.7, 7.8)
3⁗	4.19 dd (8.7, 8.7)	4.24 dd (8.7, 8.7)	4.26 dd (9.0, 9.0)	4.25 dd (8.7, 8.7)
4⁗	4.14 dd (8.7, 8.7)	4.23 dd (8.7, 8.7)	4.23 dd (9.0, 9.0)	4.23 dd (8.7, 8.7)
5⁗	4.06 m	3.95 m	3.97 ddd (9.0, 5.4, 2.4)	3.95 ddd (8.7, 5.4, 2.4)
6⁗a	4.84 dd (11.0, 1.9)	4.56 dd (11.6, 2.5)	4.57 dd (12.0, 2.4)	4.56 dd (11.8, 2.4)
b	4.31 dd (11.0, 5.4)	4.38 dd (11.6, 5.4)	4.39 dd (12.0, 5.4)	4.40 dd (11.8, 5.4)
position	Glc (III)			
1⁗′	5.10 d (7.8)			
2⁗′	4.05 dd (8.7, 7.8)			
3⁗′	4.22 dd (8.7, 8.7)			
4⁗′	4.26 dd (8.7, 8.7)			
5⁗′	3.92 ddd (8.7, 5.3, 2.3)			
6⁗′a	4.51 dd (11.9, 2.3)			
b	4.38 dd (11.9, 5.3)			

[a]^{1}H NMR spectra of **13**, **14**, and **16** were recorded at 500 MHz, and **15** was recorded at 600 MHz.

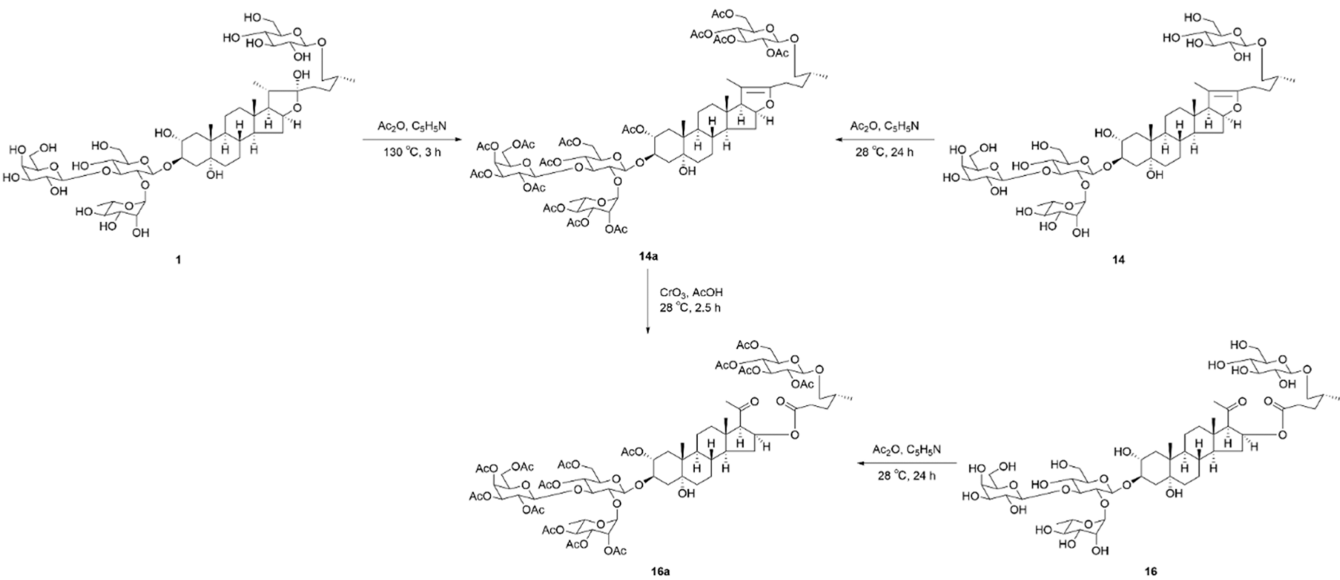

Figure 3. Chemical transformations of **1**, **14**, and **16**.

(DAPI) and observed under a fluorescence microscope. SBC-3 cells treated with **1** showed morphological changes characteristic of apoptotic cells, such as nuclear chromatin condensation and the formation of apoptotic bodies (Figure 7).

Cell cycle analysis of SBC-3 cells treated with **1** was performed. After the SBC-3 cells were incubated with **1** for 3, 6, 12, and 24 h, they were stained with PI and analyzed using a flow cytometer. After 12 h of treatment with **1**, the populations in the G_2/M phase in the P5 area and sub-G_1 peak in the P2 area were elevated to 32 ± 0.12 and 11 ± 0.36% for **1** compared to 19 ± 0.35 and 3.4 ± 0.12% for the vehicle control, respectively (Figure 8). Furthermore, the sub-G_1 peak population of SBC-3 cells treated with **1** for 24 h was significantly higher than that of SBC-3 cells treated with the vehicle control (**1**: 22 ± 0.19%; vehicle control: 6.0 ± 0.13%). Thus, **1** arrested the cell cycle of SBC-3 cells in the G_2/M phase and induced apoptotic cell death.

The activation of cysteine aspartate-specific protease (caspase) and cleavage of poly(ADP-ribose) polymerases (PARP) are hallmarks of apoptosis.[22] To detect the activation of caspases and cleavage of PARP during apoptosis induced by **1**, Western blotting analysis was conducted. After SBC-3 cells were treated with **1** for 24 h, proteins were extracted and subjected to Western blotting analysis. As shown in Figure 9, activation of caspase-3, -8, and -9, and cleavage of PARP were observed.

Two major apoptosis-inducing pathways are commonly recognized: intrinsic and extrinsic. The intrinsic pathway, also known as the mitochondrial pathway, is involved in the activation of caspase-9.[23] As caspase-9 was activated in SBC-3 cells treated with **1**, the mitochondrial membrane potential was evaluated using the 5,5′,6,6′-tetrachloro-1,1′,3,3′-tetraethylbenzimidazolylcarbocyanine iodide (JC-1) staining assay. JC-1 is widely used in apoptosis studies to monitor the mitochondrial health. In the early stages of apoptosis, mitochondrial membrane potential is depolarized. When cells are stained with JC-1 dye, at high mitochondrial membrane potentials, the dye accumulates in the mitochondria and the dye aggregates exhibit a red to red-colored fluorescent emission. At low mitochondrial membrane potentials, the concentration of JC-1 is low and it exists

https://doi.org/10.1021/acsomega.2c07766
ACS Omega 2023, 8, 2808−2830

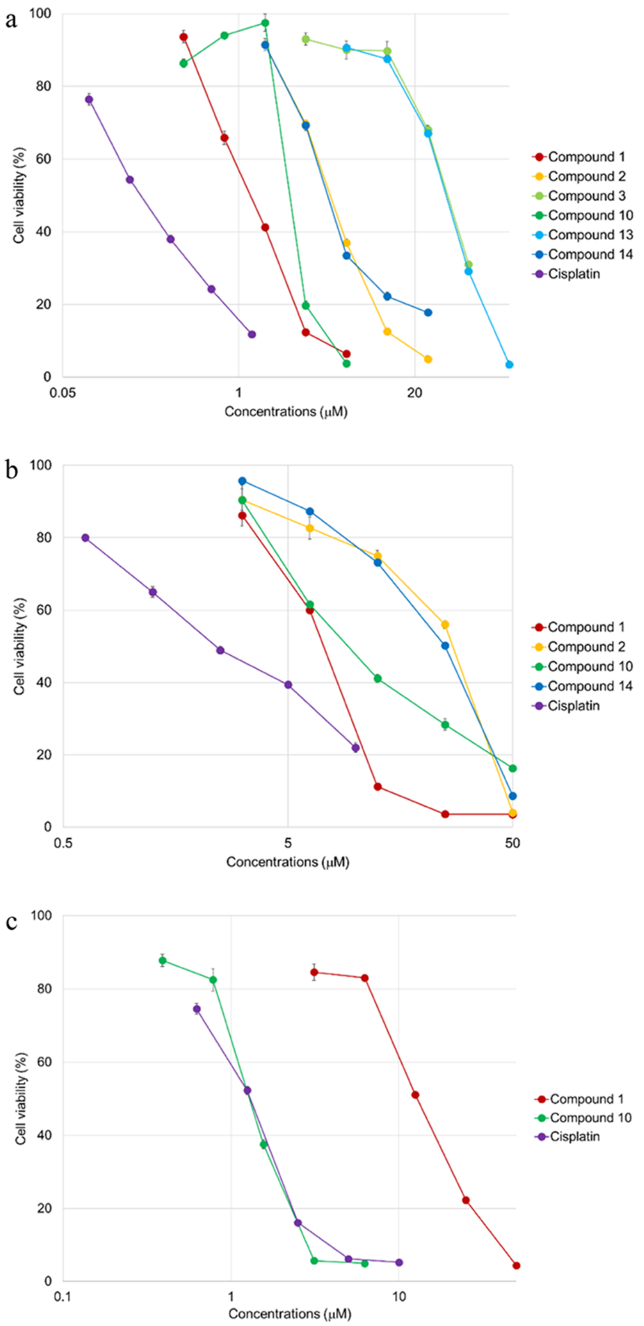

Figure 4. Dose−response curves of **1**−**3**, **10**, **13**, **14**, and cisplatin. (a) SBC-3 cells were treated with **1**−**3**, **10**, **13**, **14**, or cisplatin for 72 h. (b) A549 cells were treated with **1**, **2**, **10**, **14**, or cisplatin for 72 h. (c) HL-60 cells were treated with **1**, **10**, or cisplatin for 72 h. The cell viability was evaluated using the modified MTT assay.

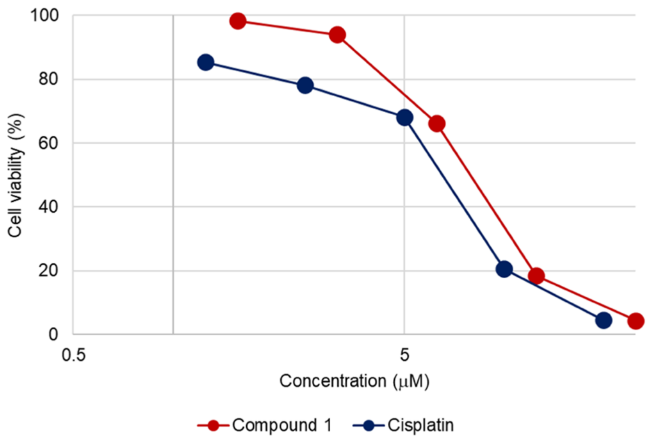

Figure 5. Dose−response curves of **1** and cisplatin. SBC-3 cells were exposed to either **1** or cisplatin for 24 h, and the cell viability was evaluated using the modified MTT assay.

predominantly as a monomer, displaying green fluorescence with emission. The mitochondrial membrane potential of SBC-3 cells treated with **1** for 3, 6, 12, and 24 h was evaluated by flow cytometry. After 12 h of treatment with **1**, the population of the mitochondrial membrane potential depolarized cells increased compared to that observed in the vehicle control (Figure 10). Next, the expression levels of Bcl-2 and Bax were evaluated using Western blotting. Bax and Bcl-2 belong to the Bcl-2 protein family and regulate the intrinsic apoptotic pathway. Bcl-2 is an antiapoptotic protein, whereas Bax acts as a pro-apoptotic effector.[24] In SBC-3 cells exposed to **1**, the protein level of Bcl-2 was significantly decreased, and the ratio of Bcl-2/Bax was lower than that in the vehicle control (Figure 11). These data suggest that **1** induces mitochondrial dysfunction in SBC-3 cells.

Reactive oxygen species (ROS), such as superoxide anions, hydrogen peroxide, hydroxyl radicals, and singlet oxygen, play important roles in diverse organisms. ROS have been reported to participate in apoptosis, and ROS accumulation causes typical apoptotic phenomena. Furthermore, mitochondria are a major ROS-producing organelle.[25] ROS generation was evaluated in SBC-3 cells treated with 5 mM *N*-acetylcysteine (NAC) as a negative control (antioxidant), 50 μM *tert*-butyl hydroperoxide (TBHP) as a positive control, cisplatin, or **1** for 3, 6, 12, and 24 h. Subsequently, SBC-3 cells were stained with 750 nM CellROX Green and analyzed using a flow cytometer. ROS generation was significantly increased in SBC-3 cells treated with either cisplatin or **1** compared to that in the vehicle control (Figure 12). As expected, intracellular ROS production in SBC-3 cells pre-treated with NAC followed by treatment with either cisplatin or **1** declined (Figure 12). Next, the influence of NAC on the apoptosis-inducing activities of cisplatin and **1** in SBC-3 cells was examined using flow cytometry. When SBC-3 cells were treated with a combination of NAC and cisplatin, the population of apoptotic cells dramatically decreased compared to those treated with cisplatin alone. In contrast, NAC had no effect on the apoptosis-inducing activity of **1** in SBC-3 cells (Figures 13 and 14). The above results implied that ROS were involved in the apoptosis-inducing activity of cisplatin in SBC-3 cells, whereas ROS generation in SBC-3 cells was due to mitochondrial dysfunction induced by **1**.

As **1** induced mitochondrial dysfunction in SBC-3 cells, the morphology of mitochondria in **1**-treated SBC-3 cells was also examined. After the SBC-3 cells were exposed to **1** for 24 h, the mitochondria were stained with MitoTracker and observed using confocal microscopy. As a result, the perimeter of the mitochondria was longer and circularity was lower than that of the vehicle control (Figure 15). Solidity indicates the degree of uneven mitochondria, and fewer dents indicate a solidity value closer to 1.0. As shown in Figure 15, the average solidity value of the mitochondria was lower than that of the vehicle control. The above data showed that the morphology of mitochondria in **1**-treated SBC-3 cells was larger, longer, and rougher than that of the vehicle control. Additionally, it is noteworthy that the morphological changes in mitochondria in **1**-treated SBC-3 cells

https://doi.org/10.1021/acsomega.2c07766
ACS Omega 2023, 8, 2808−2830

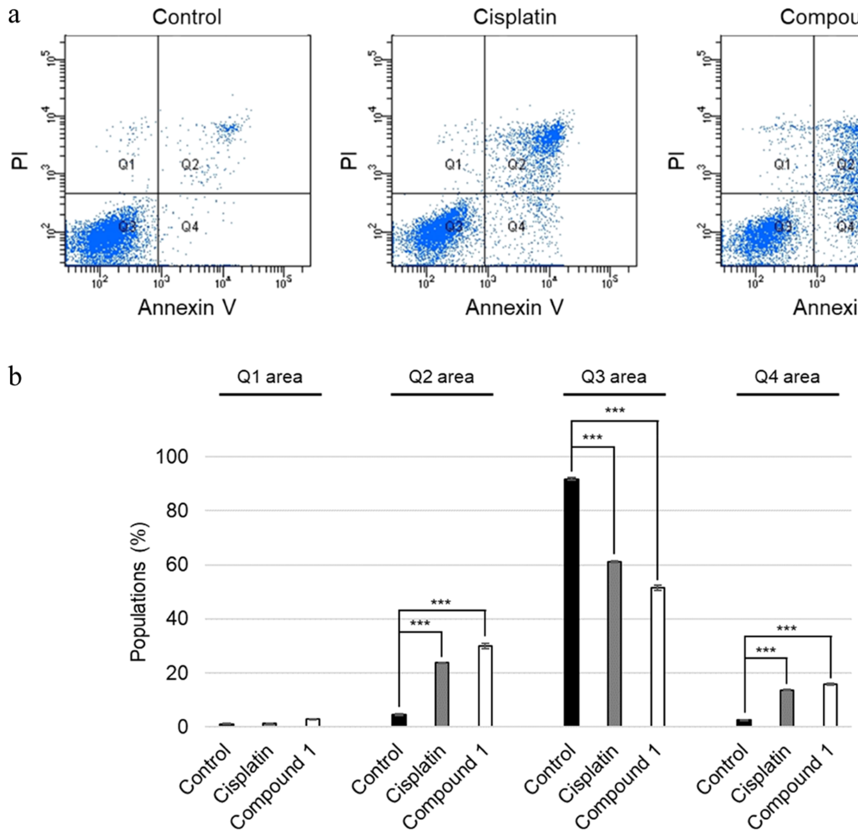

Figure 6. Detection of apoptosis in SBC-3 cells treated with either cisplatin or **1**. (a) SBC-3 cells were incubated with either 10 μM cisplatin or 15 μM **1**. After 24 h treatment, SBC-3 cells were stained with Annexin V and PI, and analyzed by a flow cytometer. (b) Bar graph shows the percentage of populations of dead cells at Q1 area, late apoptotic cells at Q2 area, live cells at Q3 area, and early apoptotic cells at Q4 area (***$p < 0.001$ vs vehicle control).

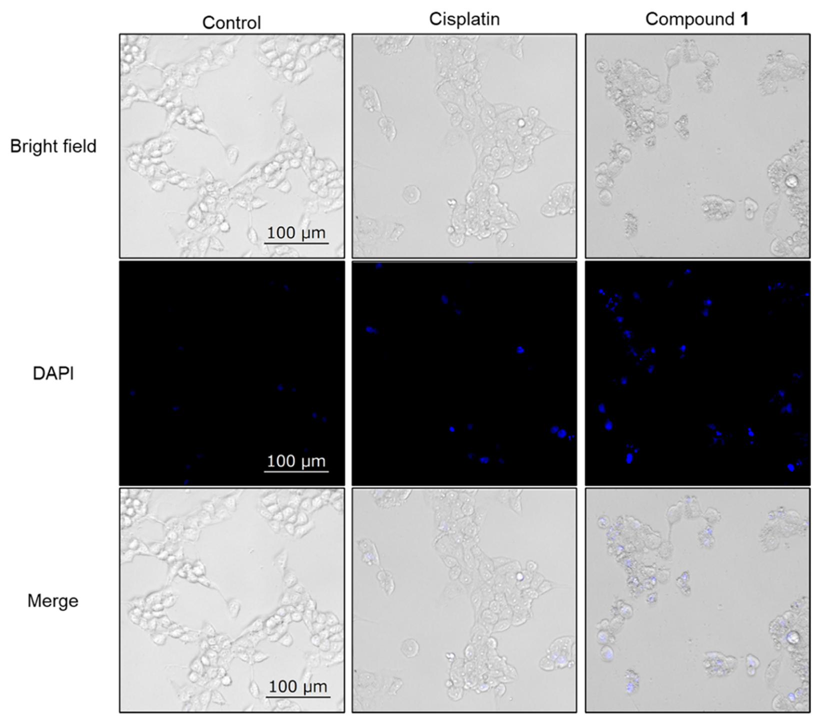

Figure 7. Morphology of SBC-3 cells treated with either cisplatin or **1**. SBC-3 cells were stained with DAPI after treatment with either 10 μM cisplatin or 15 μM **1** for 24 h, and observed using a fluorescence microscope.

tended to be opposite to those in cisplatin-treated SBC-3 cells (Figure 15).

https://doi.org/10.1021/acsomega.2c07766
ACS Omega 2023, 8, 2808−2830

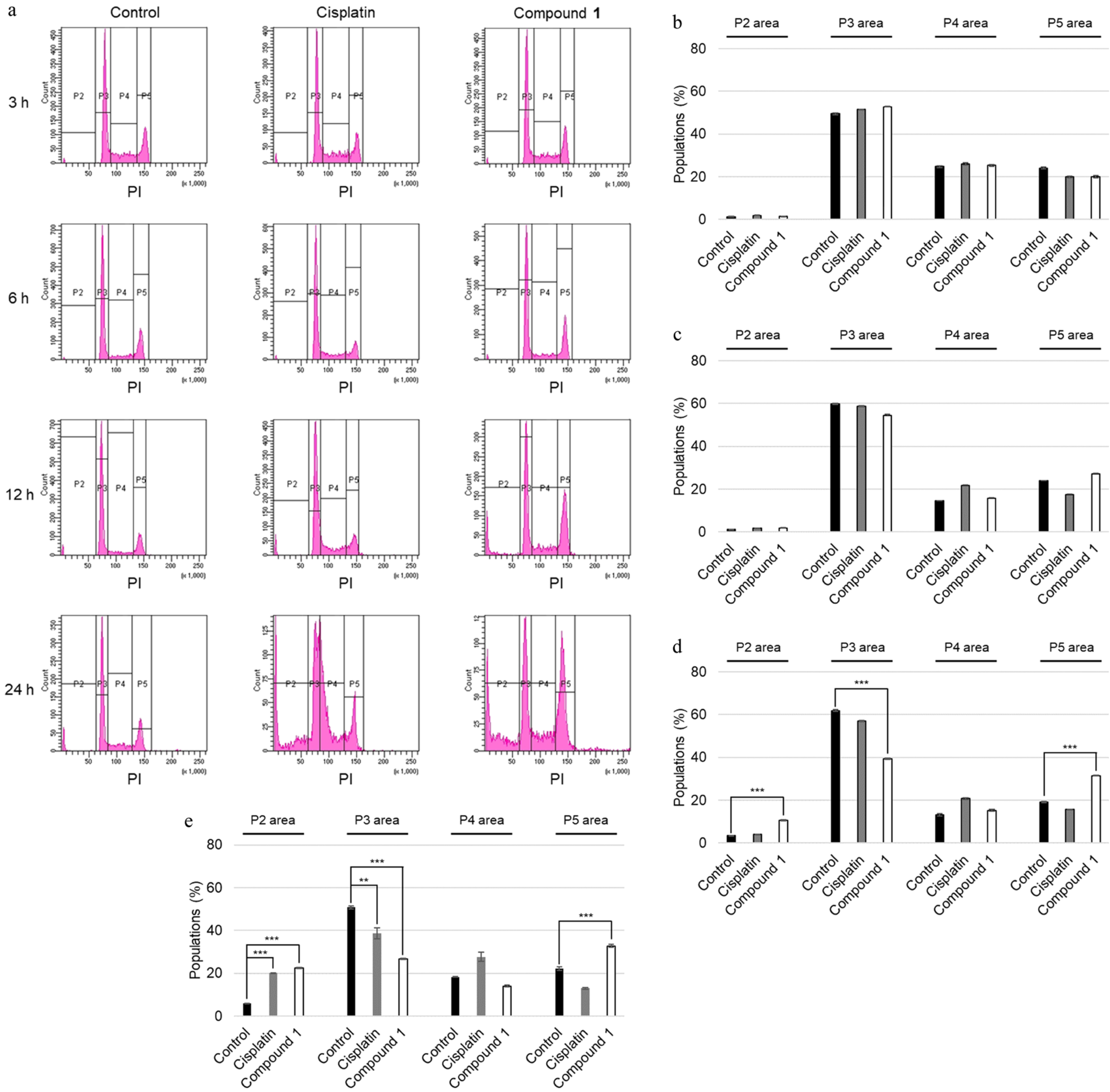

Figure 8. Effects of cisplatin and **1** on cell cycle of SBC-3 cells. (a) SBC-3 cells were treated with either 10 μM cisplatin or 15 μM **1** for 3, 6, 12, and 24 h. After treatment, SBC-3 cells were stained with PI and the DNA contents were analyzed using a flow cytometer. (b−e) Cell population percentages in the sub-G_1 (P2 area), G_0/G_1 (P3 area), S (P4 area), and G_2/M (P5 area) phases are displayed as the mean ± S.E.M. of three experiments for 3 (b), 6 (c), 12 (d), and 24 (e) h treatments (***$p < 0.001$ vs vehicle control, **$p < 0.01$ vs vehicle control).

■ EXPERIMENTAL SECTION

General Experimental Procedures. Optical rotations and infrared (IR) spectral data were measured using a P-1030 automatic digital polarimeter and a Fourier transform infrared (FT-IR) 620 spectrometer (JASCO, Tokyo, Japan), respectively. NMR spectral data were recorded on an AVIIIHD-600 (600 MHz for ^{1}H NMR; 150 MHz for ^{13}C NMR), an AVANCEIIIHD-500 (500 MHz for ^{1}H NMR; 125 MHz for ^{13}C NMR), and a DPX-400 (400 MHz for ^{1}H NMR; 100 MHz for ^{13}C NMR) spectrometer (Bruker, Billerica, MA, USA), and a JNM-ECZ600R/M1 (600 MHz for ^{1}H NMR; 150 MHz for ^{13}C NMR) spectrometer (JEOL, Tokyo, Japan) at 300 K. Chemical shifts were presented as δ values with reference to tetramethylsilane as an internal standard. HRESITOFMS data were collected using a Waters Micromass LCT mass spectrometer (Milford, MA, USA). Diaion HP-20 porous polymer polystyrene resin (Mitsubishi-Chemical, Tokyo, Japan), silica gel Chromatorex BW-300 (Fuji-Silysia Chemical, Aichi, Japan), and ODS silica gel COSMOSIL 75C_{18}-OPN (Nacalai-Tesque, Kyoto, Japan) were used for CC. Thin-layer chromatography (TLC) analysis was performed by precoated silica gel 60F_{254} or RP18 F_{254}S plates (0.25 mm thick; Merck, Darmstadt, Germany). The compounds spots were detected by spraying the TLC plates with H_2SO_4/H_2O (1:9), followed by heating. The preparative HPLC system was established from an

https://doi.org/10.1021/acsomega.2c07766
ACS Omega 2023, 8, 2808−2830

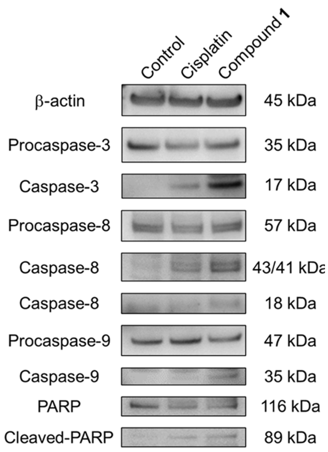

Figure 9. Detection of activated caspase-3, -8, and -9, and cleaved PARP in SBC-3 cells treated with either cisplatin or **1**. SBC-3 cells were treated with either 10 μM cisplatin or 15 μM **1** for 24 h. The extracted proteins of SBC-3 cells were applied to Western blotting analysis.

LC-20AD pump (Shimadzu, Kyoto, Japan), a Rheodyne injection port (Thermo Fisher Scientific, Waltham, MS, USA), a TSKgel ODS-100Z column (10 mm i.d. × 250 mm, 5 μm; Tosoh, Tokyo, Japan), and a RID-10A detector (Shimadzu). The following materials and reagents were adopted to the cell culture and cytotoxic activity assay: SBC-3 cells (JCRB0818), A549 cells (JCRB0076), and HL-60 cells (JCRB0085) (Human Science Research Resource Bank, Osaka, Japan); Roswell Park Memorial Institute (RPMI)-1640 medium, minimum essential medium (MEM), cisplatin, 0.25% trypsin−ethylenediaminetetraacetic acid (EDTA) solution, and fetal bovine serum (FBS) (Sigma, St. Louis, MO, USA); paraformaldehyde and phosphate-buffered saline (PBS) (FUJIFILM Wako Pure Chemical, Osaka, Japan); MTT (DOJINDO, Kumamoto, Japan); penicillin G sodium salt and streptomycin sulfate (Gibco, Gland Island, NY, USA); SH-1300 Lab microplate reader (CORONA ELECTRIC, Ibaraki, Japan); Countess II FL automated cell counter (Thermo Fisher Scientific); MCO-170AIC-PJ CO_2 incubator (PHC, Tokyo, Japan), 6-well, 48-well, and 96-well flat-bottom plates (Iwaki Glass, Chiba, Japan).

Plant Material. *A. africanus* were cultivated on the medicinal botanical garden of the Tokyo University of Pharmacy and Life Sciences in November 2017. A voucher specimen has been deposited in the herbarium of the Tokyo University of Pharmacy and Life Sciences (KS-2017-009).

Extraction and Isolation. The underground parts of *A. africanus* (24 kg) were extracted with MeOH (20 L × 2 times). The solvent was removed using an evaporator. The MeOH extract (910 g) was applied to a Diaion HP-20 column and successively eluted with MeOH/H_2O (3:7, 24 L), MeOH/H_2O (1:1, 9 L), MeOH (12 L), EtOH (6 L), and EtOAc (6 L). The MeOH/H_2O (1:1) eluted fraction (47 g) was subjected to ODS silica gel CC eluted with MeCN/H_2O (1:4) to obtain five subfractions (Frs. I−IV). Fraction I was separated by silica gel CC eluted with EtOAc/MeOH/H_2O (20:10:1; 10:10:1) to yield eight fractions (Frs. I-1−8). Fraction I-2 was divided by ODS silica gel CC eluted with MeOH/H_2O (2:3) to obtain seven fractions (Frs. I-2-1−7). Fractions I-2-2−3 were purified by ODS silica gel CC eluted with MeCN/H_2O (1:4) and MeOH/H_2O (2:3) to collect **5** (3.4 mg) and **6** (6.5 mg). Fraction I-2-6 was separated by ODS silica gel CC eluted with MeCN/H_2O (1:4) and preparative ODS HPLC using MeCN/H_2O (1:4) to yield **4** (5.2 mg), **9** (33 mg), and **10** (2.3 mg). Fraction I-2-7 was purified by ODS silica gel CC eluted with MeCN/H_2O (1:4) and MeOH/H_2O (1:1), and preparative ODS HPLC using MeCN/H_2O (1:4) to afford **3** (2.1 mg). Fractions I-3−5 were divided by ODS silica gel CC eluted with MeOH/H_2O (1:1) to obtain 11 fractions (Frs. I-3-1−11). Fraction I-3-2 was subjected to ODS silica gel CC eluted with MeCN/H_2O (1:4) and MeOH/H_2O (2:3), and preparative ODS HPLC using MeOH/H_2O (2:3) to afford **7** (15 mg), **8** (17 mg), and **12** (26 mg). Fractions I-3-6−8 were chromatographed on ODS silica gel eluted with MeCN/H_2O (1:3; 1:4) and MeOH/H_2O (1:1) to collect **2** (41 mg). Fraction I-3-10 was purified by ODS silica gel CC eluted with MeOH/H_2O (1:1) to obtain **1** (9.5 g). Fractions I-6−8 were applied to ODS silica gel CC eluted with MeOH/H_2O (8:7; 1:1) and MeCN/H_2O (5:17) to afford **13** (7.3 mg). Fractions III and IV were separated by silica gel CC eluted with $CHCl_3$/MeOH/H_2O (10:10:1) to obtain 9 fractions (Frs. III-1−9). Fraction III-2 was purified by silica gel CC eluted with $CHCl_3$/MeOH/H_2O (6:5:1), and ODS silica gel CC eluted with MeCN/H_2O (5:17; 3:7; 1:3; 1:4) and MeOH/H_2O (3:2; 1:1) to collect **11** (7.9 mg) and **14** (1.4 g). Fraction III-3 was subjected to silica gel CC eluted with $CHCl_3$/MeOH/H_2O (6:5:1), and ODS silica gel CC eluted with MeCN/H_2O (1:4) and MeOH/H_2O (6:5; 1:1; 9:11) to yield **15** (3.4 mg) and **16** (12 mg).

*(25R)-26-[(β-D-Glucopyranosyl)oxy]-2α,5α,22α-trihydroxyfurostan-3β-yl O-β-D-galactopyranosyl-(1 → 3)-O-[α-L-rhamnopyranosyl-(1 → 2)]-β-D-glucopyranoside (**1**).* Amorphous solid; $[\alpha]_D^{25}$ −68.6 (*c* 0.10, MeOH); IR (film) ν_{max} 3389, 2931 cm^{-1}; ^1H and ^{13}C NMR data, see Tables 1 and 5; HRESITOFMS *m/z* 1121.5343 $[M + Na]^+$ (calcd for $C_{51}H_{86}NaO_{25}$, 1121.5356).

*(25R)-26-[(β-D-Glucopyranosyl)oxy]-2α,5α,22α-trihydroxyfurosta-7,9-dien-3β-yl O-β-D-galactopyranosyl-(1 → 3)-O-[α-L-rhamnopyranosyl-(1 → 2)]-β-D-glucopyranoside (**2**).* Amorphous solid; $[\alpha]_D^{25}$ −29.4 (*c* 0.10, MeOH); UV (MeOH) λ_{max} (log ε): 243 (3.95), 203 (3.60) nm; IR (film) ν_{max} 3387, 2930 cm^{-1}; ^1H and ^{13}C NMR data, see Tables 1 and 5; HRESITOFMS *m/z*: 1117.5018 $[M + Na]^+$ (calcd for $C_{51}H_{82}NaO_{25}$, 1117.5043).

*(25R)-26-[(β-D-Glucopyranosyl)oxy]-2α,5α,22α-trihydroxyfurostan-3β-yl O-α-L-rhamnopyranosyl-(1 → 2)-β-D-glucopyranoside (**3**).* Amorphous solid; $[\alpha]_D^{25}$ −81.3 (*c* 0.05, MeOH); IR (film) ν_{max}: 3389, 2927 cm^{-1}; ^1H and ^{13}C NMR data, see Tables 1 and 5; HRESITOFMS *m/z*: 959.4820 $[M + Na]^+$ (calcd for $C_{45}H_{76}NaO_{20}$, 959.4828).

*(25R)-26-[(β-D-Glucopyranosyl)oxy]-2α,5α,9α,22α-tetrahydroxyfurostan-3β-yl O-α-L-rhamnopyranosyl-(1 → 2)-β-D-glucopyranoside (**4**).* Amorphous solid; $[\alpha]_D^{25}$ 4.12 (*c* 0.05, MeOH); IR (film) ν_{max}: 3375, 2928 cm^{-1}; ^1H and ^{13}C NMR data, see Tables 1 and 5; HRESITOFMS *m/z*: 975.4763 $[M + Na]^+$ (calcd for $C_{45}H_{76}NaO_{21}$, 975.4777).

*(23S,25S)-2α,5α,9α,23,25-Pentahydroxyspirostan-3β-yl O-α-L-rhamnopyranosyl-(1 → 2)-β-D-glucopyranoside (**5**).* Amorphous solid; $[\alpha]_D^{25}$ 11.5 (*c* 0.05, MeOH); IR (film) ν_{max}: 3357, 2925 cm^{-1}; ^1H and ^{13}C NMR data, see Tables 2 and 5; HRESITOFMS *m/z*: 827.4048 $[M + Na]^+$ (calcd for $C_{39}H_{64}NaO_{17}$, 827.4041).

*(23S,25S)-2α,5α,23,25-Tetrahydroxyspirostan-3β-yl O-α-L-rhamnopyranosyl-(1 → 2)-β-D-glucopyranoside (**6**).* Amorphous solid; $[\alpha]_D^{25}$ −32.5 (*c* 0.10, MeOH); IR (film) ν_{max}: 3348, 2926 cm^{-1}; ^1H and ^{13}C NMR data, see Tables 2 and 5;

https://doi.org/10.1021/acsomega.2c07766
ACS Omega 2023, 8, 2808−2830

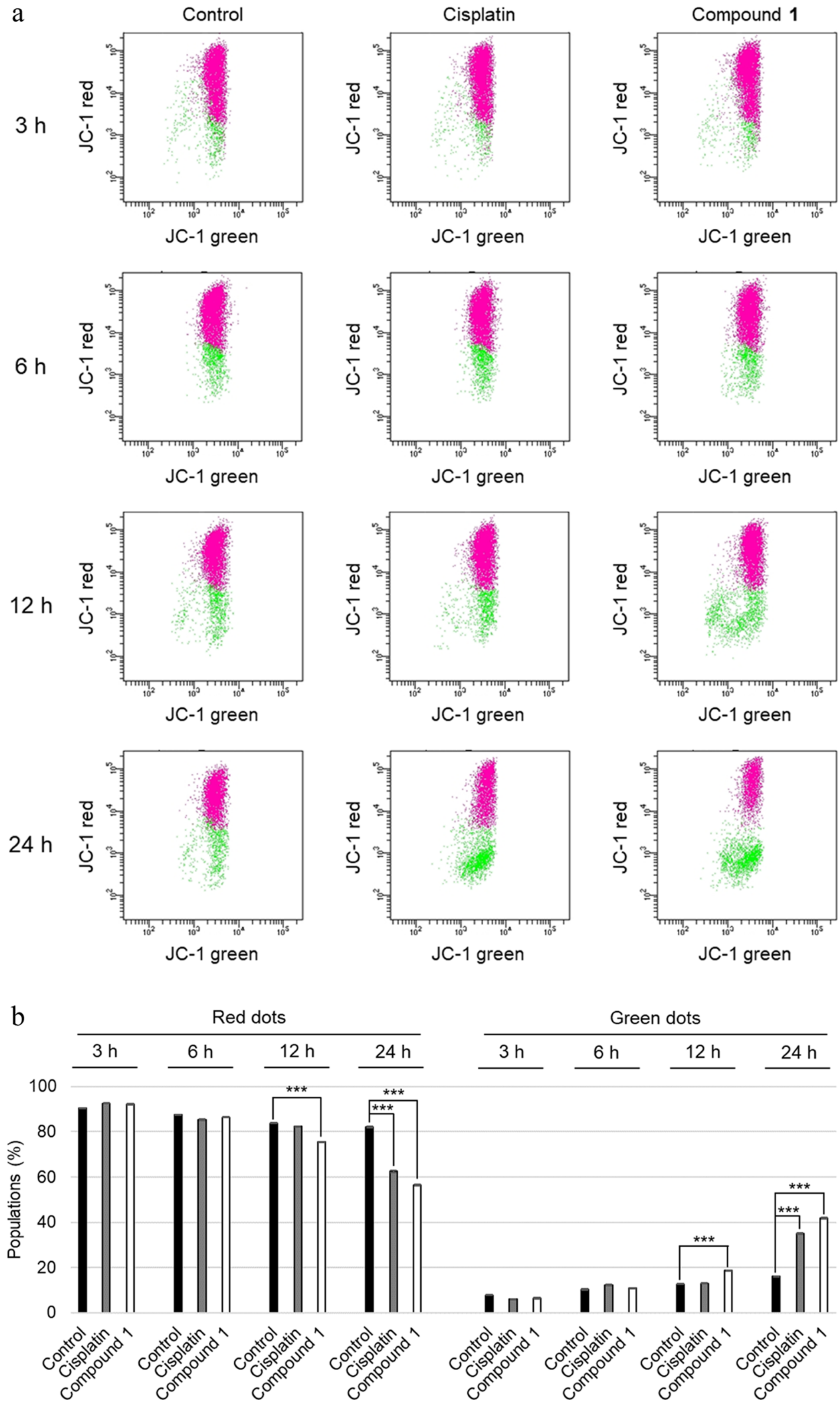

Figure 10. Detection of mitochondrial membrane potential in SBC-3 cells exposed to either cisplatin or **1**. (a) SBC-3 cells were treated with either 10 μM cisplatin or 15 μM **1** for 3, 6, 12, and 24 h. After treatment, SBC-3 cells were stained with JC-1 and analyzed using a flow cytometer. Red dots indicate the mitochondria membrane potential polarized cells, and green dots indicate mitochondria membrane depolarized cells. (b) Population percentages of mitochondria membrane potential polarized and depolarized cells are displayed as the mean ± S.E.M. of three experiments (***p < 0.001 vs vehicle control).

HRESITOFMS m/z: 811.4086 $[M + Na]^+$ (calcd for $C_{39}H_{64}NaO_{16}$, 811.4092).

(23S,25S)-2α,5α,9α,23,25-Pentahydroxyspirostan-3β-yl O-β-D-galactopyranosyl-(1 → 3)-O-[α-L-rhamnopyranosyl-(1

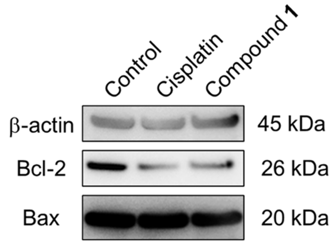

Figure 11. Detection of Bcl-2 and Bax in SBC-3 cells incubated with either cisplatin or **1**. SBC-3 cells were treated with either 10 μM cisplatin or 15 μM **1** for 24 h. The extracted proteins of SBC-3 cells were applied to Western blotting analysis.

*→ 2)]-β-D-glucopyranoside (**7**).* Amorphous solid; $[\alpha]_D^{25}$ −42.2 (*c* 0.10, MeOH); IR (film) ν_{max}: 3376, 2930 cm^{-1}; ^{1}H and ^{13}C NMR data, see Tables 2 and 6; HRESITOFMS *m/z*: 989.4561 [M + Na]$^+$ (calcd for $C_{45}H_{74}NaO_{22}$, 989.4569).

*(23S,25S)-2α,5α,23,25-Tetrahydroxyspirostan-3β-yl O-β-D-galactopyranosyl-(1 → 3)-O-[α-L-rhamnopyranosyl-(1 → 2)]-β-D-glucopyranoside (**8**).* Amorphous solid; $[\alpha]_D^{25}$ −42.1 (*c* 0.10, MeOH); IR (film) ν_{max}: 3376, 2928 cm^{-1}; ^{1}H and ^{13}C NMR data, see Tables 2 and 6; HRESITOFMS *m/z*: 973.4610 [M + Na]$^+$ (calcd for $C_{45}H_{74}NaO_{21}$, 973.4620).

*(24S,25S)-24-[(β-D-Glucopyranosyl)oxy]-2α,5α-dihydroxyspirostan-3β-yl O-α-L-rhamnopyranosyl-(1 → 2)-β-D-glucopyranoside (**9**).* Amorphous solid; $[\alpha]_D^{25}$ −39.4 (*c* 0.05, MeOH); IR (film) ν_{max}: 3376, 2927 cm^{-1}; ^{1}H and ^{13}C NMR data, see Tables 3 and 6; HRESITOFMS *m/z*: 957.4667 [M + Na]$^+$ (calcd for $C_{45}H_{74}NaO_{20}$, 957.4671).

*(24S,25S)-24-[(β-D-Glucopyranosyl)oxy]-2α,5α-dihydroxyspirost-7-en-3β-yl O-α-L-rhamnopyranosyl-(1 → 2)-β-D-glucopyranoside (**10**).* Amorphous solid; $[\alpha]_D^{25}$ −52.2 (*c* 0.05, MeOH); IR (film) ν_{max}: 3376, 2927 cm^{-1}; ^{1}H and ^{13}C NMR data, see Tables 3 and 6; HRESITOFMS *m/z*: 955.4513 [M + Na]$^+$ (calcd for $C_{45}H_{72}NaO_{20}$, 955.4515).

*(24S,25S)-24-[(β-D-Glucopyranosyl)oxy]-2α,5α-dihydroxyspirostan-3β-yl O-β-D-galactopyranosyl-(1 → 3)-O-[α-L-rhamnopyranosyl-(1 → 2)]-β-D-glucopyranoside (**11**).* Amorphous solid; $[\alpha]_D^{25}$ −48.6 (*c* 0.05, MeOH); IR (film) ν_{max}: 3390, 2931 cm^{-1}; ^{1}H and ^{13}C NMR data, see Tables 3 and 6; HRESITOFMS *m/z*: 1119.5176 [M + Na]$^+$ (calcd for $C_{51}H_{84}NaO_{25}$, 1119.5199).

*(24S,25S)-24-[(β-D-Glucopyranosyl)oxy]-2α,5α,9α-trihydroxyspirostan-3β-yl O-β-D-galactopyranosyl-(1 → 3)-O-[α-L-rhamnopyranosyl-(1 → 2)]-β-D-glucopyranoside (**12**).* Amorphous solid; $[\alpha]_D^{25}$ −37.0 (*c* 0.10, MeOH); IR (film) ν_{max}: 3388, 2929 cm^{-1}; ^{1}H and ^{13}C NMR data, see Tables 3 and 6; HRESITOFMS *m/z*: 1135.5139 [M + Na]$^+$ (calcd for $C_{51}H_{84}NaO_{26}$, 1135.5149).

*(25S)-27-[O-β-D-Glucopyranosyl-(1 → 6)-(β-D-glucopyranosyl)oxy]-2α,5α-dihydroxyspirost-7-en-3β-yl O-β-D-galactopyranosyl-(1 → 3)-O-[α-L-rhamnopyranosyl-(1 → 2)]-β-D-glucopyranoside (**13**).* Amorphous solid; $[\alpha]_D^{25}$ −40.4 (*c* 0.05, MeOH); IR (film) ν_{max}: 3389, 2930 cm^{-1}; ^{1}H and ^{13}C NMR data, see Tables 4 and 7; HRESITOFMS *m/z*: 1279.5570 [M + Na]$^+$ (calcd for $C_{57}H_{92}NaO_{30}$, 1279.5571).

*(25R)-26-[(β-D-Glucopyranosyl)oxy]-2α,5α-dihydroxyfurost-20(22)-en-3β-yl O-β-D-galactopyranosyl-(1 → 3)-O-[α-L-rhamnopyranosyl-(1 → 2)]-β-D-glucopyranoside (**14**).* Amorphous solid; $[\alpha]_D^{25}$ −26.2 (*c* 0.05, MeOH); IR (film) ν_{max}: 3390, 2931 cm^{-1}; ^{1}H and ^{13}C NMR data, see Tables 4 and 7; HRESITOFMS *m/z*: 1079.5249 [M − H]$^-$ (calcd for $C_{51}H_{83}O_{24}$, 1079.5274).

*Tetradecaacetate of **14** (**14a**).* ^{1}H NMR (400 MHz, C_5D_5N) δ_H 1.62 (3H, s, H-21), 1.34 (3H, s, H-19), 0.93 (3H, d, *J* = 6.6 Hz, H-27), 0.77 (3H, s, H-18), and 2.28−1.94 (each s, Ac × 14). HRESITOFMS *m/z*: 1691.6675 [M + Na]$^+$ (calcd for $C_{79}H_{112}NaO_{38}$, 1691.6729).

*(25R)-26-[(β-D-Glucopyranosyl)oxy]-2α,5α,23-trihydroxyfurost-20(22)-en-3β-yl O-β-D-galactopyranosyl-(1 → 3)-O-[α-L-rhamnopyranosyl-(1 → 2)]-β-D-glucopyranoside (**15**).* Amorphous solid; $[\alpha]_D^{25}$ −36.6 (*c* 0.05, MeOH); IR (film) ν_{max}: 3390, 2930 cm^{-1}; ^{1}H and ^{13}C NMR data, see Tables 4 and 7; HRESITOFMS *m/z*: 1119.5182 [M + Na]$^+$ (calcd for $C_{51}H_{84}NaO_{25}$, 1119.5199).

*3β-[(O-β-D-Galactopyranosyl-(1 → 3)-O-[α-L-rhamnopyranosyl-(1 → 2)]-β-D-glucopyranosyl)oxy]-2α,5α-dihydroxy-16β-[[(4R)-5-(β-D-glucopyranosyl)oxy-4-methyl-1-oxopentyl]oxy]-pregn-5-en-20-one (**16**).* Amorphous solid; $[\alpha]_D^{25}$ −27.0 (*c* 0.05, MeOH); IR (film) ν_{max}: 3389, 2933, and 1714 cm^{-1}; ^{1}H and ^{13}C NMR data, see Tables 4 and 7; HRESITOFMS *m/z*: 1135.5123 [M + Na]$^+$ (calcd for $C_{51}H_{84}NaO_{26}$, 1135.5149).

*Tetradecaacetate of **16** (**16a**).* ^{1}H NMR (400 MHz, C_5D_5N) δ_H 2.10 (3H, s, H-21), 1.25 (3H, s, H-18), 0.95 (3H, s, H-19), 0.85 (3H, d, *J* = 6.6 Hz, H-27), and 2.30−1.95 (s, Ac × 14). HRESITOFMS *m/z*: 1723.6545 [M + Na]$^+$ (calcd for $C_{79}H_{112}NaO_{40}$, 1723.6628).

Enzymatic Hydrolysis of 1 and 2. Compounds **1** and **2** were independently produced by enzymatic hydrolysis. Compounds **1** (30 mg) and **2** (8.4 mg) were treated with β-D-glucosidase (EC 3.2.1.21; Sigma) (**1**: 30 mg; **2**: 10 mg) in AcOH/AcOK buffer (pH 5.0, 2.0 mL) at 28 °C for 39 h (**1**) and for 24 h (**2**). Each reaction mixture was chromatographed on an ODS silica gel column eluted with MeOH/H_2O (**1**: 7:3; **2**: 3:1) to afford agapanthussaponin A (16 mg) from **1** and agapanthussaponin C (3.2 mg) from **2**, and sugar fractions (**1**: 2.0 mg; **2**: 0.40 mg). Each sugar fraction was analyzed using HPLC under the following conditions: pump, DP-8020 (Tosoh); detector, Shodex OR-2 (Showa-Denko, Tokyo, Japan); column, Capcell Pak NH_2 UG80 (4.6 mm × 250 mm, 5 μm; Shiseido, Tokyo, Japan); solvent, MeCN/H_2O (17:3); flow rate, 1.0 mL/min. D-Glucose was identified by comparing the retention time (t_R) and optical rotation with those of the authentic sample: D-glucose (13.3, positive optical rotation).

Acetylation of 1, 14, and 16. Compound **1** (100 mg) was adopted to acetylation with Ac_2O (2.0 mL) in pyridine (2.0 mL) at 130 °C for 3 h. The reaction mixture was purified by silica gel CC eluted with *n*-hexane/EtOAc (1:2) to obtain **14a** (42 mg). Compounds **14** (50 mg) and **16** (5.0 mg) were independently applied to acetylation with Ac_2O (2.0 mL) in pyridine (2.0 mL) at 28 °C for 24 h. The reaction mixture of **14** was chromatographed on silica gel CC eluted with *n*-hexane/EtOAc (1:2) to afford the corresponding tetradecaacetate of **14** (**14a**; 35 mg). The reaction mixture of **16** was purified by ODS silica gel CC eluted with MeCN/H_2O (3:1) to obtain the corresponding tetradecaacetate of **16** (**16a**; 4.0 mg).

Oxidation with CrO_3 of 14a. A CrO_3 (15 mg) solution in AcOH/H_2O (19:1, 1.0 mL) was added to **14a** (10 mg), which was then dissolved in AcOH/H_2O (19:1, 2.0 mL). After the solution was stirred at 28 °C for 2.5 h, the excess CrO_3 in the solution was decomposed by adding MeOH (3.0 mL). The reaction mixture was purified by ODS silica gel eluted with MeCN/H_2O (3:1) to collect **16a** (1.5 mg).

https://doi.org/10.1021/acsomega.2c07766
ACS Omega 2023, 8, 2808−2830

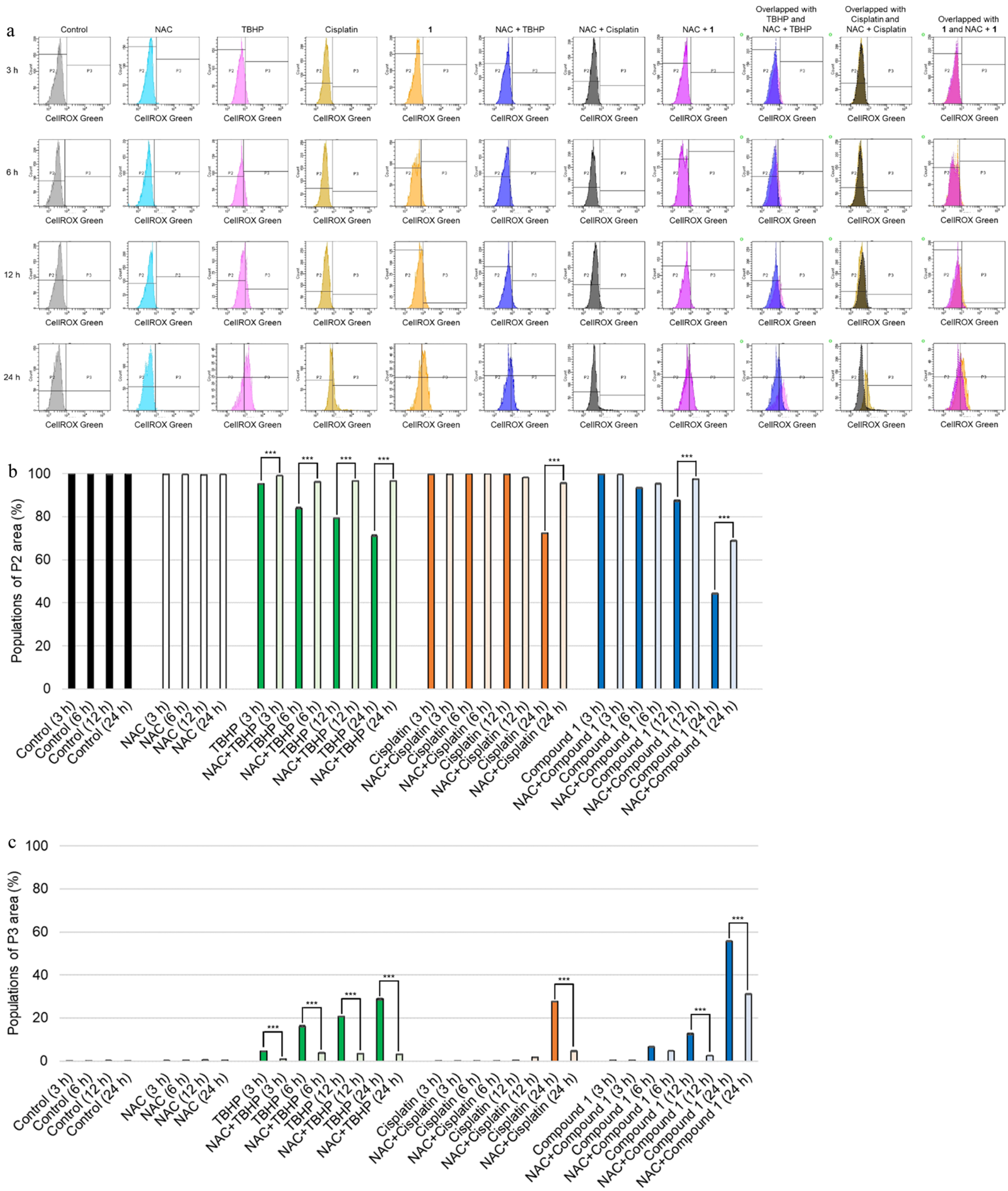

Figure 12. ROS generation in SBC-3 cells treated with NAC, TBHP, cisplatin, or **1**. (a) SBC-3 cells were treated with 5 mM NAC, 50 μM TBHP, 10 μM cisplatin, or 15 μM **1** for 3, 6, 12, and 24 h. After treatment, SBC-3 cells were stained with CellROX Green and ROS generation levels were evaluated using a flow cytometer. (b, c) Population percentage of SBC-3 cells in the P2 area and P3 area are displayed as the mean ± S.E.M. of three experiments (***p < 0.001 vs vehicle control).

Acid Hydrolysis of 9 and 13. Compounds **9** (5.0 mg) and **13** (3.0 mg) were independently dissolved in 1 M HCl (dioxane/H_2O, 1:1) and heated at 95 °C for 2 h under an Ar atmosphere. Each reaction mixture was neutralized by passing through an Amberlite IRA-96 (Organo, Tokyo, Japan) column and separated by ODS silica gel CC eluted with MeCN/H_2O

https://doi.org/10.1021/acsomega.2c07766
ACS Omega 2023, 8, 2808−2830

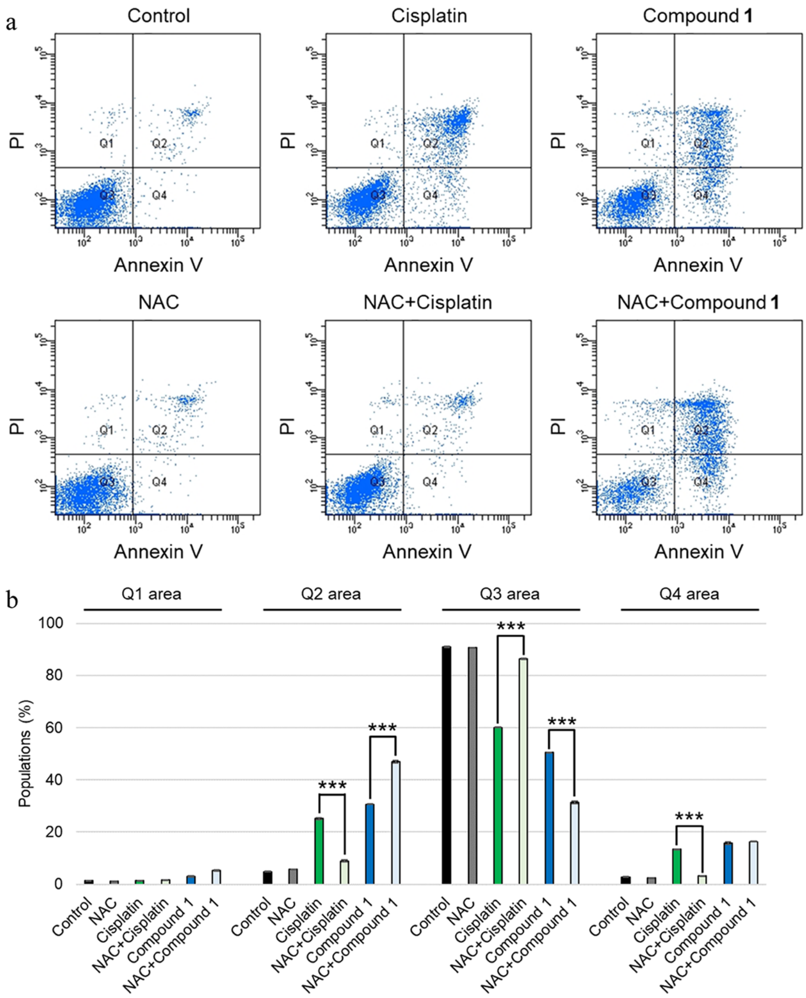

Figure 13. Detection of apoptosis in SBC-3 cells treated with NAC, cisplatin, **1**, a combination of NAC and cisplatin, or a combination of NAC and **1**. (a) SBC-3 cells were treated with 5 mM NAC, 10 μM cisplatin, 15 μM **1**, a combination of 5 mM NAC and 10 μM cisplatin, or a combination of 5 mM NAC and 15 μM **1** for 24 h. After treatment, SBC-3 cells were stained with Annexin V and PI, and analyzed by a flow cytometer. (b) Bar graph for the percentage of populations of Q1 area, Q2 area, Q3 area, and Q4 area (***p < 0.001 vs vehicle control).

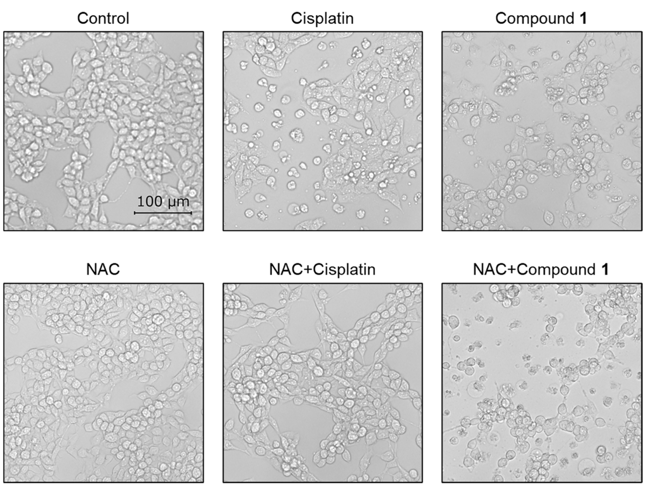

Figure 14. Morphology of SBC-3 cells treated with NAC, cisplatin, **1**, a combination of NAC and cisplatin, or a combination of NAC and **1**. SBC-3 cells were exposed to 5 mM NAC, 10 μM cisplatin, 15 μM **1**, a combination of 5 mM NAC and 10 μM cisplatin, or a combination of 5 mM NAC and 15 μM **1** for 24 h, and observed by a microscope.

(1:3) to afford sugar fractions (1.8 mg from **9**; 1.3 mg from **13**). HPLC analysis of each sugar fraction was carried out under the same conditions as those of **1** and **2**, except for the flow rate (0.5 mL/min). D-Glucose in **9** and **13**, L-rhamnose in **9** and **13**, and D-galactose in **13** were identified by comparing their retention times (t_R) and optical rotations with those of authentic samples: L-rhamnose (16.3, negative optical rotation), D-galactose (32.7, positive optical rotation), and D-glucose (33.6, positive optical rotation).

Cell Culture and Cytotoxic Activity Assay. SBC-3 and A549 cells were maintained in MEM, and HL-60 cells were kept in RPMI-1640 medium including 10% heat-inactive FBS supplemented with L-glutamine, 100 μg/mL streptomycin sulfate, and 100 unit/mL penicillin G sodium salt. After incubation with each test sample for 72 h, the cell viability was measured with the MTT assay method as previously described.[26] A dose−response curve was plotted for each compound, **1**−**3**, **10**, **13**, and **14**, which inhibited cell growth by more than 50% at sample concentrations of 50 μM, and the concentrations at which 50% inhibition (IC_{50}) of cell growth occurred were calculated. The cell growth inhibition of SBC-3 cells (cell concentration: 5×10^4 cells/mL) exposed to **1** for 24 h was elucidated by the same method as above (Table 8).

https://doi.org/10.1021/acsomega.2c07766
ACS Omega 2023, 8, 2808−2830

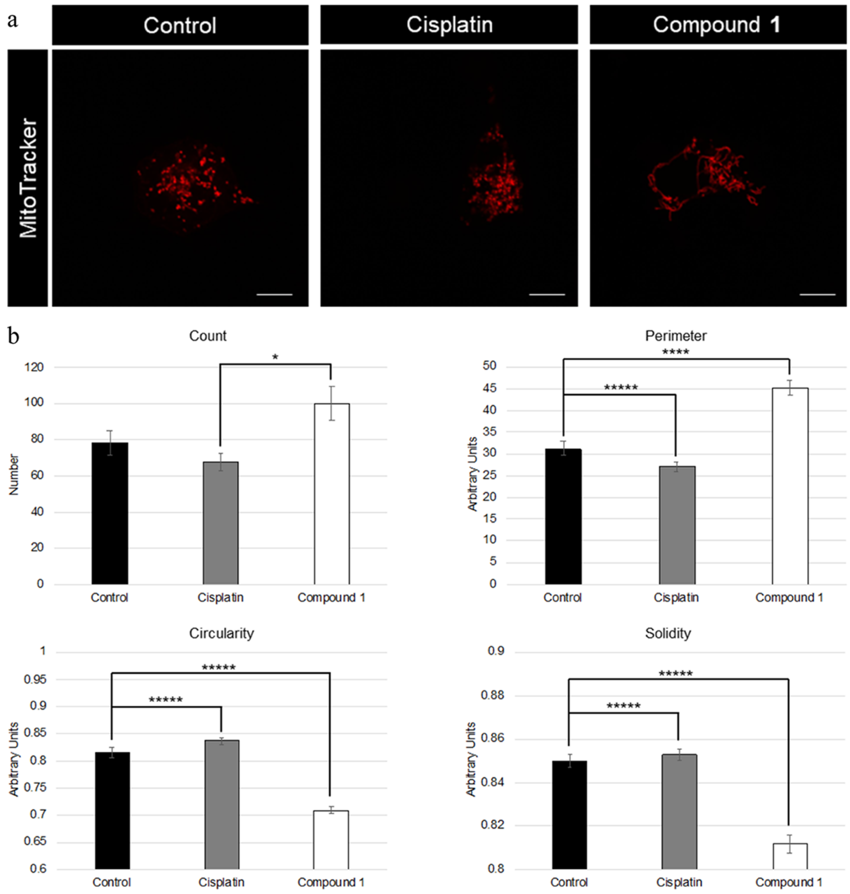

Figure 15. Mitochondria morphology in SBC-3 cells treated with cisplatin or **1**. (a) SBC-3 cells were treated with exposure to either 10 μM cisplatin or 15 μM **1** for 24 h. After treatment, mitochondria were stained with MitoTracker and observed using confocal microscopy. (b) Number of mitochondria, mitochondria perimeter, mitochondria circularity, and mitochondria solidity were analyzed by the ImageJ Macro Tool (*p < 0.05, ****p < 0.0005, *****p < 0.0001 vs vehicle control). The scale bars indicate 10 μm.

Double Staining with Annexin V and PI. SBC-3 cells (cell concentration: 5×10^5 cells/mL) were cultured in a six-well flat-bottom plate. After preincubation for 24 h, SBC-3 cells were treated with EtOH/H_2O (1:1) as control, 10 μM cisplatin, or 15 μM **1** for 24 h. The double staining with Annexin V and PI procedure was previously described.[26] The flow cytometry analysis was performed using a BD FACSCelesta flow cytometer (BD Biosciences, Franklin Lakes, NJ, USA).

DAPI Staining and Morphology Observation. SBC-3 cells (cell concentration: 2×10^5 cells/mL) were harvested in a 48-well flat-bottom plate. After preincubation for 24 h, SBC-3 cells were treated with EtOH/H_2O (1:1), 10 μM cisplatin, or 15 μM **1**. After 24 h treatment, SBC-3 cells were fixed with 1% glutaraldehyde at 28 °C for 30 min. Then, SBC-3 cells were rinsed with PBS and stained with DAPI (0.5 μg/mL dissolved in PBS) at 28 °C for 10 min. The morphology of SBC-3 cells was observed using a BZ-X710 All-in-One Fluorescence Microscope (KEYENCE, Osaka, Japan).

Analysis of Cell Cycle. SBC-3 cells (cell concentration: 5×10^5 cells/mL) were seeded in a six-well flat-bottom plate. After preincubation for 24 h, SBC-3 cells were treated with EtOH/H_2O (1:1), 10 μM cisplatin, or 15 μM **1** for 3, 6, 12, and 24 h. The analysis of cell cycle was conducted by the same method as previously described.[26] Cell cycle distribution was analyzed by a BD FACSCelesta flow cytometer.

Western Blotting. SBC-3 cells (cell concentration: 5×10^5 cells/mL) were cultured in a six-well flat-bottom plate and treated with EtOH/H_2O (1:1), 10 μM cisplatin, or 15 μM **1** for 24 h. The Western blotting analysis was carried out by the same procedures as previously reported.[26] The following antibodies were recruited: β-actin (8H10D10 Mouse mAb, product number 3700, 1:1000; Cell Signaling Technology, Danvers, MA, USA), caspase-8 (1C12 Mouse mAb, product number 9746, 1:1000; Cell Signaling Technology), caspase-9 (C9 Mouse mAb, product number 9508, 1:2000; Cell Signaling Technology), caspase-3 (3G2 Mouse mAb, product number 9668, 1:1000, Cell Signaling Technology), PARP (46D11 Rabbit mAb, product number 9532, 1:1000; Cell Signaling Technology), Bax (2D2 Mouse mAb, product number 89477, 1:1000; Cell Signaling Technology), Bcl-2 (124 Mouse mAb, product number 15071, 1:1000; Cell Signaling Technology), anti-rabbit IgG, horseradish peroxidase (HRP)-linked antibody (product number 7074, 1:10000; Cell Signaling Technology), and anti-mouse IgG, HRP-linked antibody (product number 7076, 1:10000; Cell Signaling Technology). The signals were detected using ECL Prime Western Blotting Detection Reagents (GE Healthcare, Boston, MA, USA), and photographed by a LAS-3000 luminescent image analyzer (FUJIFILM, Tokyo, Japan).

Detection of Mitochondria Membrane Potential. SBC-3 cells (cell concentration 5×10^5 cells/mL) were harvested in a six-well flat-bottom plate. After preincubation for 24 h, SBC-3 cells were treated with EtOH/H_2O (1:1), 10 μM cisplatin, or 15 μM **1** for 3, 6, 12, and 24 h. The mitochondria membrane

https://doi.org/10.1021/acsomega.2c07766
ACS Omega 2023, 8, 2808−2830

Table 5. ^{13}C NMR Spectral Data of 1−6 in C_5D_5N (δ in ppm)[a]

position	1	2	3	4	5	6
1	40.0	38.6	39.9	35.0	35.0	39.9
2	70.9	70.7	71.1	71.0	70.9	71.1
3	82.7	82.8	83.5	83.0	82.8	83.4
4	40.2	39.1	40.6	40.9	40.7	40.5
5	73.6	73.0	73.6	76.8	76.7	73.6
6	34.3	37.5	34.2	34.6	34.5	34.1
7	26.5	117.4	26.5	21.8	21.8	26.5
8	34.1	135.5	34.1	37.3	37.1	34.2
9	45.5	142.5	45.5	77.4	77.4	45.5
10	40.5	42.9	40.5	43.2	43.1	40.5
11	21.6	121.1	21.6	28.0	28.0	21.6
12	40.4	42.5	40.4	35.4	35.6	40.6
13	41.2	41.1	41.2	41.3	41.5	41.5
14	56.2	51.6	56.2	48.7	48.8	56.2
15	32.4	31.7	32.4	32.2	31.9	32.1
16	81.1	81.3	81.1	81.3	82.0	81.9
17	63.9	63.0	63.9	63.9	62.5	62.6
18	16.8	16.1	16.8	16.0	16.1	16.9
19	17.2	26.3	17.2	20.2	20.1	17.2
20	40.6	40.9	40.6	40.7	35.7	35.7
21	16.4	15.9	16.3	16.4	14.7	14.8
22	110.6	110.7	110.6	110.6	112.0	112.0
23	37.1	36.9	37.1	37.2	64.5	64.5
24	28.3	28.3	28.3	28.3	43.4	43.4
25	34.2	34.2	34.2	34.2	69.8	69.8
26	75.2	75.2	75.2	75.3	69.1	69.1
27	17.4	17.4	17.4	17.4	26.8	26.8
position	Glc (I)	Glc (I)	Glc (I)	Glc (I)	Glc	Glc
1′	100.7	101.1	101.6	101.4	101.2	101.5
2′	77.1	76.9	77.8	77.8	77.8	77.9
3′	89.1	89.1	79.4	79.5	79.4	79.4
4′	69.6	69.5	71.7	71.7	71.7	71.7
5′	77.7	77.6	78.1	78.2	78.1	78.1
6′	62.1	62.0	62.3	62.3	62.3	62.3
position	Rha	Rha	Rha	Rha	Rha	Rha
1″	102.1	102.1	102.0	102.0	102.0	102.0
2″	72.3	72.3	72.3	72.4	72.3	72.3
3″	72.7	72.6	72.7	72.7	72.7	72.7
4″	74.0	74.1	74.1	74.1	74.1	74.1
5″	69.5	69.4	69.4	69.4	69.3	69.4
6″	18.5	18.6	18.5	18.5	18.5	18.5
position	Gal	Gal	Glc (II)	Glc (II)		
1‴	105.1	105.1	104.8	104.9		
2‴	72.4	72.4	75.1	75.2		
3‴	75.1	75.2	78.5	78.6		
4‴	69.9	70.0	71.6	71.6		
5‴	77.3	77.4	78.4	78.4		
6‴	62.0	62.0	62.7	62.7		
position	Glc (II)	Glc (II)				
1⁗	104.8	104.8				
2⁗	75.2	75.1				
3⁗	78.5	78.5				
4⁗	71.6	71.6				
5⁗	78.4	78.4				
6⁗	62.7	62.7				

[a] ^{13}C NMR spectra of **1**−**3** and **6** were recorded at 125 MHz, and **4** and **5** were recorded at 150 MHz.

Table 6. ^{13}C NMR Spectral Data of 7−12 in C_5D_5N (δ in ppm)[a]

position	7	8	9	10	11	12
1	35.0	40.0	39.9	40.3	40.0	35.0
2	70.7	70.9	71.1	70.6	70.9	70.7
3	82.1	82.6	83.4	83.1	82.8	82.0
4	40.4	40.2	40.6	40.1	40.3	40.4
5	76.7	73.5	73.6	73.0	73.6	76.7
6	34.6	34.1	34.1	37.0	34.3	34.6
7	21.8	26.6	26.5	115.9	26.5	21.7
8	37.1	34.3	34.2	138.8	34.2	37.2
9	77.4	45.5	45.4	43.3	45.5	77.2
10	43.1	40.5	40.5	39.8	40.5	43.1
11	28.0	21.6	21.6	21.5	21.6	27.9
12	35.6	40.6	40.2	39.5	40.3	35.2
13	41.5	41.5	40.8	41.6	40.9	40.9
14	48.8	56.3	56.2	54.9	56.2	48.8
15	32.0	32.1	31.9	31.3	32.0	31.8
16	82.0	81.9	81.6	81.3	81.6	81.7
17	62.6	62.6	62.5	62.1	62.6	62.5
18	16.1	16.9	16.6	16.4	16.6	15.8
19	20.1	17.2	17.2	19.0	17.3	20.1
20	35.7	35.7	42.0	42.5	42.1	42.0
21	14.7	14.8	14.7	14.7	14.8	14.8
22	112.0	112.0	111.5	111.6	111.5	111.5
23	64.5	64.5	40.7	40.7	40.9	40.8
24	43.4	43.4	81.5	81.5	81.6	81.5
25	69.8	69.8	38.1	38.1	38.2	38.1
26	69.1	69.1	65.0	65.0	65.1	65.0
27	26.8	26.8	13.4	13.4	13.5	13.4
position	Glc	Glc	Glc (I)	Glc (I)	Glc (I)	Glc (I)
1′	100.5	100.7	101.5	101.5	100.8	100.5
2′	77.0	77.1	77.8	77.7	77.1	77.0
3′	89.0	89.2	79.4	79.4	89.3	89.0
4′	69.6	69.6	71.7	71.6	69.6	69.6
5′	77.7	77.7	78.1	78.1	77.8	77.7
6′	62.1	62.1	62.3	62.2	62.2	62.1
position	Rha	Rha	Rha	Rha	Rha	Rha
1″	102.1	102.1	102.0	102.0	102.2	102.1
2″	72.2	72.3	72.3	72.3	72.3	72.2
3″	72.6	72.7	72.7	72.7	72.7	72.6
4″	74.0	74.0	74.1	74.1	74.1	74.0
5″	69.4	69.5	69.4	69.4	69.5	69.4
6″	18.5	18.5	18.5	18.5	18.6	18.5
position	Gal	Gal	Glc (II)	Glc (II)	Gal	Gal
1‴	105.1	105.1	106.3	106.3	105.1	105.1
2‴	72.4	72.4	75.6	75.6	72.4	72.4
3‴	75.1	75.2	78.5	78.5	75.2	75.2
4‴	69.9	69.9	71.6	71.5	70.0	69.9
5‴	77.3	77.3	78.0	78.0	77.4	77.3
6‴	62.0	62.0	62.7	62.7	62.0	62.0
position					Glc (II)	Glc (II)
1⁗					106.4	106.3
2⁗					75.6	75.6
3⁗					78.6	78.5
4⁗					71.7	71.6
5⁗					78.0	78.0
6⁗					62.8	62.7

[a] ^{13}C NMR spectra of **8**, **10**, and **11** were recorded at 125 MHz, and **7**, **9**, and **12** were recorded at 150 MHz.

https://doi.org/10.1021/acsomega.2c07766
ACS Omega 2023, 8, 2808−2830

Table 7. ^{13}C NMR Spectral Data of 13−16 in C_5D_5N (δ in ppm)[a]

position	13	14	15	16
1	40.3	40.0	40.0	40.0
2	70.4	70.9	70.9	70.9
3	82.5	82.6	82.8	82.8
4	39.8	40.2	40.4	40.3
5	73.0	73.5	73.5	73.6
6	37.1	34.2	34.3	34.3
7	115.9	26.6	26.7	26.2
8	139.0	33.9	33.9	33.5
9	43.4	45.5	45.5	45.6
10	39.8	40.5	40.5	40.5
11	21.6	21.8	21.8	21.2
12	39.6	40.1	40.1	38.5
13	41.6	43.8	43.9	42.8
14	55.0	54.5	54.5	53.7
15	31.4	34.4	34.4	35.4
16	80.9	84.5	84.6	74.8
17	62.6	64.6	64.9	66.8
18	16.4	14.4	14.6	14.0
19	19.0	17.2	17.3	17.2
20	42.4	103.6	105.0	205.5
21	14.8	11.7	11.6	30.4
22	109.5	152.2	154.3	173.2
23	31.2	23.6	63.7	32.3
24	23.8	31.4	39.6	29.0
25	36.6	33.4	30.9	33.4
26	63.7	74.9	75.5	74.7
27	72.1	17.3	17.8	16.9
position	Glc (I)	Glc (I)	Glc (I)	Glc (I)
1′	100.8	100.7	100.8	100.8
2′	77.0	77.1	77.1	77.1
3′	89.1	89.1	89.3	89.2
4′	69.5	69.6	69.6	69.6
5′	77.7	77.6	77.8	77.8
6′	62.1	62.1	62.2	62.2
position	Rha	Rha	Rha	Rha
1″	102.1	102.1	102.2	102.1
2″	72.3	72.3	72.4	72.3
3″	72.7	72.6	72.7	72.7
4″	74.1	74.0	74.1	74.1
5″	69.4	69.5	69.5	69.5
6″	18.5	18.5	18.6	18.6
position	Gal	Gal	Gal	Gal
1‴	105.1	105.0	105.2	105.1
2‴	72.4	72.4	72.4	72.4
3‴	75.3	75.1	75.3	75.2
4‴	70.0	69.9	70.0	70.0
5‴	77.4	77.3	77.4	77.4
6‴	62.0	62.0	62.0	62.0
position	Glc (II)	Glc (II)	Glc (II)	Glc (II)
1⁗	104.9	104.8	105.1	104.9
2⁗	75.0	75.1	75.2	75.1
3⁗	78.5	78.5	78.6	78.6
4⁗	71.5	71.6	71.8	71.7
5⁗	77.2	78.4	78.5	78.5
6⁗	70.1	62.8	62.9	62.8
position	Glc (III)			
1⁗′	105.4			
2⁗′	75.2			
3⁗′	78.4			
4⁗′	71.6			
5⁗′	78.5			
6⁗′	62.7			

[a]^{13}C NMR spectra of **13**, **14**, and **16** were recorded at 125 MHz, and **15** was recorded at 150 MHz.

Table 8. Cytotoxic Activities of 1−16 against SBC-3, A549, and HL-60 Cells[a]

	IC$_{50}$ (μM)		
compounds	SBC-3	A549	HL-60
1	1.2 ± 0.010	7.2 ± 0.061	13 ± 0.088
2	4.7 ± 0.063	27 ± 0.33	>50
3	35 ± 0.29	>50	>50
4	>50	>50	>50
5	>50	>50	>50
6	>50	>50	>50
7	>50	>50	>50
8	>50	>50	>50
9	>50	>50	>50
10	2.4 ± 0.030	9.3 ± 0.12	1.3 ± 0.025
11	>50	>50	>50
12	>50	>50	>50
13	34 ± 0.73	>50	>50
14	4.5 ± 0.059	25 ± 0.29	>50
15	>50	>50	>50
16	>50	>50	>50
cisplatin	0.19 ± 0.00088	2.4 ± 0.15	1.3 ± 0.012

[a]Data are represented as the mean value ± standard error of the mean (S.E.M.) of the three experiments performed in triplicate.

potential was detected by the same procedures as previously described.[26] Finally, SBC-3 cells were analyzed using a BD FACSCelesta flow cytometer.

Evaluation of ROS Generation Level. SBC-3 cells (cell concentration 5×10^5 cells/mL) were cultured in a six-well flat-bottom plate and preincubated for 24 h. Then, SBC-3 cells were treated with EtOH/H_2O (1:1), 5 mM NAC, 50 μM TBHP, 10 μM cisplatin, or 15 μM **1** for 3, 6, 12, and 24 h. The ROS generation levels were measured using the same methods as previously described.[26] The ROS generation levels were evaluated using a BD FACSCelesta flow cytometer.

Observation of Mitochondria Morphology. SBC-3 cells were seeded on glass-bottom dishes. After pre-treatment with EtOH/H_2O (1:1), 10 μM cisplatin, or 15 μM **1** for 24 h, SBC-3 cells were incubated with 50 nM MitoTracker (Invitrogen, Waltham, MA, USA) and 1 μg/mL Calcein-AM (DOJINDO) at 37 °C for 30 min, and the staining was analyzed using an FV3000 confocal microscope (OLYMPUS, Tokyo, Japan). ImageJ Macro Tool was utilized for the analysis of mitochondrial morphology.[27] Briefly, the image was first converted to binary by thresholding. The parameters on morphologies of mitochondrial structures, including mitochondria number, perimeter, circularity, and solidity, were calculated using the ImageJ Macro software.

Statistical Analysis. Statistical analyses of the detection of apoptosis, analysis of the cell cycle, detection of mitochondrial membrane potential, and evaluation of ROS generation were carried out by a one-way analysis of variance (ANOVA) followed by Dunnett's test. Statistical analysis of mitochondria morphology was conducted by ANOVA followed by Tukey's test.

■ ASSOCIATED CONTENT

Supporting Information

The Supporting Information is available free of charge at https://pubs.acs.org/doi/10.1021/acsomega.2c07766.

MS data, IR, UV, and NMR spectra of **1−16** (PDF)

■ AUTHOR INFORMATION

Corresponding Author

Tomoki Iguchi − *Department of Medicinal Pharmacognosy, School of Pharmacy, Tokyo University of Pharmacy and Life Sciences, Hachioji, Tokyo 192-0392, Japan*; orcid.org/0000-0003-0337-9776; Email: iguchit@toyaku.ac.jp

Authors

Naoki Takahashi − *Department of Medicinal Pharmacognosy, School of Pharmacy, Tokyo University of Pharmacy and Life Sciences, Hachioji, Tokyo 192-0392, Japan*

Anju Nagamine − *Department of Medicinal Pharmacognosy, School of Pharmacy, Tokyo University of Pharmacy and Life Sciences, Hachioji, Tokyo 192-0392, Japan*

Remina Shirai − *Laboratory of Molecular Neurology, School of Life Science, Tokyo University of Pharmacy and Life Sciences, Hachioji, Tokyo 192-0392, Japan*

Akihiro Nagata − *Department of Medicinal Pharmacognosy, School of Pharmacy, Tokyo University of Pharmacy and Life Sciences, Hachioji, Tokyo 192-0392, Japan*

Junji Yamauchi − *Laboratory of Molecular Neurology, School of Life Science, Tokyo University of Pharmacy and Life Sciences, Hachioji, Tokyo 192-0392, Japan; Department of Pharmacology, National Research Institute for Child Health and Development, Setagaya, Tokyo 157-8535, Japan*

Yoshihiro Mimaki − *Department of Medicinal Pharmacognosy, School of Pharmacy, Tokyo University of Pharmacy and Life Sciences, Hachioji, Tokyo 192-0392, Japan*

Complete contact information is available at: https://pubs.acs.org/10.1021/acsomega.2c07766

Author Contributions

The manuscript was written through contributions of all authors. All authors have given approval to the final version of the manuscript.

Funding

This research was financially supported in part by the Japan Society for the Promotion of Sciences (JSPS) KAKENHI Grant Number 22K15306.

Notes

The authors declare no competing financial interest.

■ ACKNOWLEDGMENTS

The authors thank Dr. Akihito Yokosuka for technical assistance with the experiments.

■ ABBREVIATIONS

ANOVA, analysis of variance; caspase, cysteine aspartate-specific protease; CC, column chromatography; COSY, correlation spectroscopy; DALY, disability-adjusted life year; DAPI, 4′,6′-diamidino-2-phenylindole dichloride; EDTA, ethylenediaminetetraacetic acid; FBS, fetal bovine serum; FDA, Food and Drug Administration; FT-IR, Fourier transform infrared; HMBC, heteronuclear multiple bond correlation; HPLC, high-performance liquid chromatography; HRESITOFMS, high-resolution electrospray ionization time-of-flight mass spectroscopy; HSQC, heteronuclear multiple quantum coherence; IR, infrared; JC-1, 5,5′,6,6′-tetrachloro-1,1′,3,3′-tetraethylbenzimidazolylcarbocyanine iodide; MEM, minimum essential medium; MTT, 3-(4,5-dimethylthiazol-2-yl)-2,5-diphenyl-2-tetrazolium bromide; NAC, *N*-acetylcysteine; NMR, nuclear magnetic resonance; NOE, nuclear Overhauser effect; NOESY, nuclear Overhauser and exchange spectroscopy; ODS, octadecylsilanized; PARP, poly(ADP-ribose) polymerases; PBS, paraformaldehyde and phosphate-buffered saline; PI, propidium iodide; ROS, reactive oxygen species; TBHP, *tert*-butyl hydroperoxide; TLC, thin-layer chromatography; UV, ultraviolet

■ REFERENCES

(1) Sang, S.; Chu, C.; Zhang, T.; Chen, H.; Yang, X. The global burden of disease attributable to ambient fine particulate matter in 204 countries and territories, 1990-2019: A systematic analysis of the global burden of disease study 2019. *Ecotoxicol. Environ. Saf.* **2022**, *238*, No. 113588.

(2) Kocarnik, J. M.; Compton, K.; Dean, F. E.; et al. Cancer incidence, mortality, years of life lost, years lived with disability, and disability-adjusted life years for 29 cancer groups from 2010 to 2019. *JAMA Oncol.* **2022**, *8*, 420−444.

(3) Newman, D. J.; Cragg, G. M. Natural products as source of new drugs over the nearly four decades from 01/1981 to 09/2019. *J. Nat. Prod.* **2022**, *83*, 770−803.

(4) Mimaki, Y.; Watanabe, K.; Sakagami, H.; Sashida, Y. Steroidal glycosides from the leaves of *Cestrum nocturnum*. *J. Nat. Prod.* **2002**, *65*, 1863−1868.

(5) Kuroda, M.; Mimaki, Y.; Ori, K.; Sakagami, H.; Sashida, Y. Steroidal glycosides from the bulbs of *Ornithogalum thyrsoides*. *J. Nat. Prod.* **2004**, *67*, 1690−1696.

(6) Kuroda, M.; Ori, K.; Takayama, H.; Sakagami, H.; Mimaki, Y.; Karataviosides, G.-K. five new bisdesmosidic steroidal glycosides from the bulbs of *Allium karataviense*. *Steroids* **2015**, *93*, 96−104.

(7) Yokosuka, A.; Suzuki, T.; Tatsuno, S.; Mimaki, Y. Steroidal glycosides from the underground parts of *Yucca glauca* and their cytotoxic activities. *Phytochemistry* **2014**, *101*, 109−115.

(8) Tang, L.; Wang, Z.; Wu, H.; Yokosuka, A.; Mimaki, Y. Steroidal glycosides from the underground parts of *Dracaena thalioides* and their cytotoxic activity. *Phytochemistry* **2014**, *107*, 102−110.

(9) Iguchi, T.; Kuroda, M.; Naito, R.; Watanabe, T.; Matsuo, Y.; Yokosuka, A.; Mimaki, Y. Structural characterization of cholestane rhamnosides from *Ornithogalum saundersiae* bulbs and their cytotoxic activity against cultured tumor cells. *Molecules* **2017**, *22*, No. 1243.

(10) Matsuo, Y.; Shinoda, D.; Nakamaru, A.; Kamohara, K.; Sakagami, H.; Mimaki, Y. Steroidal glycosides from *Convallaria majalis* whole plants and their cytotoxic activity. *Int. J. Mol. Sci.* **2017**, *18*, No. 2358.

(11) Iguchi, T.; Uchida, Y.; Takano, S.; Yokosuka, A.; Mimaki, Y. Novel steroidal glycosides from the whole plants of *Helleborus foetidus*. *Chem. Pharm. Bull.* **2020**, *68*, 273−287.

(12) Iguchi, T.; Kuroda, M.; Ishihara, M.; Sakagami, H.; Mimaki, Y. Steroidal constituents isolated from the seeds of *Withania somnifera*. *Nat. Prod. Res.* **2021**, *35*, 2205−2210.

(13) Tatsuno, S.; Iguchi, T.; Kuroda, M.; Ishihara, M.; Sakagami, H.; Mimaki, Y. A new and 23 known cardenolide glycosides from *Thevetia neriifolia* seeds and their cytotoxic activities against human oral carcinoma cell lines. *Nat. Prod. Res.* **2021**, *35*, 4388−4393.

(14) Yokosuka, A.; Ishihara, K.; Yamada, T.; Iguchi, T.; Mimaki, Y. Steroidal glycosides from the aerial parts of *Avena sativa* L. and their cytotoxic activity. *J. Agric. Food Chem.* **2021**, *69*, 14568−14579.

(15) Matsuo, Y.; Tsuchihashi, H.; Takatori, K.; Fukaya, H.; Kuroda, M.; Mimaki, Y. Cytotoxic triterpene and steroidal glycosides from the seeds of *Digitalis purpurea* and synergistic cytotoxicity of steroidal glycosides and etoposide in SBC-3 cells. *Bioorg. Chem.* **2022**, *122*, No. 105697.

(16) Kamara, B. I.; Manong, D. T. L.; Brandt, E. V. Isolation and synthesis of a dimeric dihydrochalcone from *Agapanthus africanus*. *Phytochemistry* **2005**, *66*, 1126−1132.

(17) Miyahara, T.; Takahashi, M.; Ozeki, Y.; Sasaki, N. Isolations of an acyl-glucose-dependent anthocyanin 7-*O*-glucosyltransferase from the monocot *Agapanthus africanus*. *J. Plant Physiol.* **2012**, *169*, 1321−1326.

(18) Veale, D. J. H.; Havlik, I.; Oliver, D. W.; Dekker, T. G. Pharmacological effects of *Agapanthus africanus* on the isolated rat uterus. *J. Ethnopharmacol.* **1999**, *66*, 257−262.

(19) Singh, D. N.; Verma, N.; Raghuwanshi, S.; Shukla, P. K.; Kulshreshtha, D. K. Antifungal activity of *Agapanthus africanus* extractives. *Fitoterapia* **2008**, *79*, 298−300.

(20) Nakamura, O.; Mimaki, Y.; Sashida, Y.; Nikaido, T.; Ohmoto, T. Agapanthussaponins A-D, new potent cAMP phosphodiesterase inhibitors from the underground parts of *Agapanthus inapertus*. *Chem. Pharm. Bull.* **1993**, *41*, 1784−1789.

(21) Chen, G.; Liu, T.; Lu, X.; Wang, H. F.; Hua, H. M.; Pei, Y. H. New steroidal glycosides from *Tribulus terrestris* L. *J. Asian Nat. Prod. Res.* **2012**, *14*, 780−784.

(22) Okubo, S.; Ohta, T.; Shoyama, Y.; Uto, T. Steroidal saponins isolated from the rhizome of *Dioscorea tokoro* inhibit cell growth and autophagy in hepatocellular carcinoma cells. *Life* **2021**, *11*, No. 749.

(23) Eeva, J.; Nuutinen, U.; Ropponen, A.; Mättö, M.; Eray, M.; Pellinen, R.; Wahfors, J.; Pelkonen, J. The involvement of mitochondria and the caspase-9 activation pathway in rituximab-induced apoptosis in FL cells. *Apoptosis* **2009**, *14*, 687−698.

(24) Alam, M.; Alam, S.; Shamsi, A.; Adnan, M.; Elasbali, A. M.; Al-Soud, W. A.; Alreshidi, M.; Hawsawi, Y. M.; Tippana, A.; Pasupuleti, V. R.; Hassan, I. Bax/Bcl-2 cascade is regulated by the EGFR pathway: Therapeutic targeting of non-small cell lung cancer. *Front. Oncol.* **2022**, *12*, No. 869672.

(25) Fleury, C.; Mignotte, B.; Vayssiere, J. L. Mitochondrial reactive oxygen species in cell death signaling. *Biochimie* **2002**, *84*, 131−141.

(26) Takahashi, N.; Iguchi, T.; Kuroda, M.; Mishima, M.; Mimaki, Y. Novel oleanane-type triterpene glycosides from the *Saponaria officinalis* L. seeds and apoptosis-inducing activity via mitochondria. *Int. J. Mol. Sci.* **2022**, *23*, No. 2047.

(27) Bosch, A.; Calvo, M.Automated Quantitative Analysis of Mitochondrial Morphology. In *Computer Optimized Microscopy*; Rebollo, E.; Bosch, M., Eds.; Methods in Molecular Biology; Humana: New York, 2019; Vol. *2040*, pp 99−115.

https://doi.org/10.1021/acsomega.2c07766
ACS Omega 2023, 8, 2808−2830